Received: 25 October 2017 | Revised: 09 June 2018 | Accepted: 03 August 2018 | Published on: 25 October 2018

DOI: 10.1002/qj.3391

RESEARCH ARTICLE

Quarterly Journal of the Royal Meteorological Society RMetS

Ensemble sensitivity analysis of Greenland blocking in medium-range forecasts

Tess Parker[1] | Tim Woollings[1] | Antje Weisheimer[2,3]

[1]Department of Physics, University of Oxford, UK
[2]European Centre for Medium-Range Weather Forecasts, Reading, UK
[3]National Centre for Atmospheric Science, Department of Physics, University of Oxford, UK

Correspondence
Tess Parker, Atmospheric, Oceanic and Planetary Physics, University of Oxford, Parks Road, Oxford OX1 3PU, UK.
Email: tess.parker@physics.ox.ac.uk

The North Atlantic Oscillation (NAO) is the leading mode of variability in the large-scale circulation over the North Atlantic in winter, and strongly influences the weather and climate of Europe. On synoptic time-scales, the negative phase of the NAO often corresponds to the occurrence of a blocking episode over Greenland. Hence, the dynamics and predictability of these blocking events is of interest for the prediction of the NAO and its related impacts over a wide region.

Ensemble sensitivity analysis utilises the information contained in probabilistic forecast ensembles to calculate a statistical relationship between a forecast metric and some precursor condition. Here the method is applied to 15-day forecasts of a set of 26 Greenland blocking events using the state-of-the-art European Centre for Medium-Range Weather Forecasts (ECMWF) forecasting system. The ensemble sensitivity analysis shows that Greenland blocking does not develop in isolation in these forecasts, but instead the blocking is sensitive to remote precursors, such as 500 and 50 hPa geopotential height, particularly in the low-frequency flow. In general, there are more significant sensitivities to anomalies in the Tropics than in the polar regions. Stratospheric sensitivities tend to emerge at later lead times than tropospheric sensitivities. The strongest and most robust sensitivities correspond to a Rossby wave precursor reaching from the Pacific basin across North America.

KEYWORDS

Drought; ECMWF ensemble; Ensemble sensitivity analysis; Greenland blocking; Medium-range forecasts; NAO; Rossby waves; TIGGE

1 | INTRODUCTION

The weather and climate of Europe is strongly influenced by the large-scale circulation over the North Atlantic (e.g. Wanner *et al.*, 2001), which controls not only the mean temperature and precipitation but also their extremes, particularly in winter (e.g. Trigo *et al.*, 2004; Santos *et al.*, 2007; Kenyon and Hegerl, 2010; Efthymiadis *et al.*, 2011; Cattiaux *et al.*, 2012). The North Atlantic Oscillation (NAO) is the leading mode of variability in the North Atlantic in the wintertime, and displacements of the jet streams are the dominant source of variability in the patterns of weather in the midlatitudes (Hurrell and Deser, 2009). The NAO refers to oscillations in atmospheric pressure between the Arctic and the Atlantic at subtropical latitudes, associated with changes in mean wind speed and direction, and is most pronounced during boreal winter. The resulting changes in the position and speed of the North Atlantic jet result in changes to seasonal mean heat and moisture transport from the Atlantic to neighbouring continents, the storm track and the number and intensity of storms, sea surface temperatures, ocean currents and associated heat transport, and sea ice cover in the Arctic (Hurrell

et al., 2003). Empirical orthogonal function (EOF) analysis of the 250 hPa zonal wind field (Athanasiadis *et al.*, 2009) produces a leading EOF in the Atlantic sector that projects strongly upon the NAO, and is characterized by latitudinal shifts and pulsing of the eddy-driven jet. In the positive phase of this EOF teleconnection pattern, the storm track is anomalously strong and displaced poleward of its climatological mean position; in the negative phase, the storm track is weak and displaced equatorward.

Woollings *et al.* (2008) have shown that the NAO can be considered a measure of the variability of zonal flow over the Atlantic basin, with negative NAO periods characterized by frequent high-latitude blocking and thus weak zonal flow, and positive periods by a lack of such blocking. Similar relationships were found by Shabbar *et al.* (2001), Scherrer *et al.* (2006) and Croci-Maspoli *et al.* (2007), and in a simple model by Luo *et al.* (2007). In contrast to the quasi-stationary anticyclones that block the ambient westerly winds and associated weather systems in the midlatitudes, high-latitude blocking is characterized by an anticyclone on the poleward side of the storm track and jet stream locations, which tends to divert rather than block the westerly flow. Yet, such anticyclones are often identified as blocks by objective blocking indices. Older studies such as Watson and Colucci (2002) and Mauritsen and Källén (2004) found that blocking was generally underestimated in the models. Blocking indices that focus on a particular band of latitude (Tibaldi and Molteni, 1990; Pelly and Hoskins, 2003a) are dominated by blocking over the east Pacific Ocean and Europe, whereas more recent two-dimensional indices that cover all latitudes result in the identification of more high-latitude blocking over both the Pacific and Atlantic basins (Tibaldi *et al.*, 1994; Schwierz *et al.*, 2004; Diao *et al.*, 2006; Scherrer *et al.*, 2006; Berrisford *et al.*, 2007; Barriopedro *et al.*, 2010; Masato *et al.*, 2013b). Objective analyses of weather regimes in the North Atlantic frequently distinguish a pattern with an anticyclone poleward of the storm track near southern Greenland (Vautard, 1990; Cheng and Wallace, 1993; Kimoto and Ghil, 1993). This regime results in the diversion of the storm track and hence the axis of maximum precipitation, with regional implications for winter rainfall amounts over Europe (Santos *et al.*, 2013).

Studies focusing on NAO events suggest that the positive phase (NAO+) has clear hemispheric precursors, but that the negative phase (NAO–) develops more *in situ* (Feldstein, 1976; Franzke *et al.*, 2004; Drouard *et al.*, 2015), seemingly implying a lower potential for predictability. However, focusing on Greenland blocking episodes does reveal remote precursors to NAO–, as constructing composites around blocking onset ensures that travelling wave features are aligned (Woollings *et al.*, 2008). Furthermore, Oortwijn (1998) suggested that the onset of blocking may be an inherently sensitive flow pattern. Local diabatic processes are thought to be important in some blocking cases (Pfahl *et al.*, 2015), but here we concentrate on hemispheric circulation precursors, which provide potential for extended-range predictability. Such precursors could include anomalies in the zonal flow or the planetary or synoptic waves (e.g. Luo *et al.*, 2014). In this study, we identify high-latitude blocking episodes in the Greenland region using the two-dimensional index of Masato *et al.* (2013b), and investigate the sensitivity of such blocking to a range of potential atmospheric precursors using ensemble sensitivity analysis (e.g. Ancell and Hakim, 2007; Hakim and Torn, 2008). While based on a linear regression technique, this approach makes use of a very realistic, state-of-the-art high-resolution forecasting model. This provides the potential to learn more about the evolution and predictability of the NAO. It could also inform on the role of model biases, for example if an event is found to be sensitive to an aspect of the model with a known bias.

The data and methodology are presented in the next section. Sections 3 and 4 discuss the tropospheric and stratospheric precursors to Greenland blocking in a reanalysis dataset and the ECMWF forecasting model respectively. In section 5, a case-study of a Greenland blocking episode is presented to expand on the precursor composites and to illustrate the ensemble sensitivity method. Section 6 examines the results of the ensemble sensitivity analysis for Greenland blocking episodes for both the tropospheric and stratospheric precursors, and discusses the robustness of the results. The main conclusions are summarised in section 7.

2 | DATA AND METHODOLOGY

2.1 | Data

Reanalysis data used in this study are taken from the Interim European Centre for Medium-Range Weather Forecasts (ECMWF) Reanalysis (ERA-Interim, herein ERA-I) (Dee *et al.*, 2011), at 6-hourly time steps on a reduced N256 Gaussian grid, and were accessed through the JASMIN facility (Lawrence *et al.*, 2013). Greenland blocking episodes (GBEs, defined below) in the winter period of December–February (DJF) for the years 2006–2015 are examined (i.e. DJF 2006/07 – DJF 2014/15, or nine winters from 2007 to 2015, with winters dated by the year of the relevant January). When compositing the periods prior to onset or subsequent to decay of an episode, some days in November and March are of necessity included in the results.

The International Grand Global Ensemble (TIGGE; (Bougeault *et al.*, 2010, http://tigge.ecmwf.int/) is a World Meteorological Organization project to improve the accuracy of one-day to two-week forecasts of severe weather events. The TIGGE dataset contains ensemble forecast data from ten global numerical weather prediction (NWP) centres, from October 2006 onwards. The data used in this study are from the ECMWF TIGGE ensemble (henceforward ECMWF), based on an unperturbed control forecast and 50 members with slightly perturbed initial conditions, at 6-hourly time steps and with 0.5° resolution, for forecasts initialized both

10 and 5 days prior to the onset of a GBE. The ensemble is designed to capture a range of realistic possible outcomes at a later date, given small perturbations to the initial state conditions and the application of stochastic physics to simulate model uncertainties (Buizza *et al.*, 2008; Palmer *et al.*, 2009; Shutts *et al.*, 2011).

In this paper we use the numerical forecasts as a tool to improve our understanding of the physical system, for which we require a level of confidence in the model. Hence, while the 10-day lead forecasts present a greater ensemble spread which is of use for the sensitivity analysis, we also include results from the 5-day forecasts for comparison, in which the model is more strongly constrained to be close to observations by the initial conditions. In addition, we now review literature relevant to the skill of the model in representing the physical system in question.

A shift from deterministic NWP, based on single numerical integrations, to a probabilistic approach in which ensembles of integrations produce the probability distribution function of forecast states, has improved the detection of predictive signals and provided a framework for extending forecast length beyond 10 days (Buizza and Leutbecher, 2015). Forecast models assimilate more accurate initial conditions and observations, and model advances have improved the representation of processes and include more components, such as coupled dynamical ocean models. Ensemble forecasts provide a dynamical, flow-dependent estimate of the probability distribution of the atmospheric state at the initial and forecast times. In their assessment of the ECMWF ensemble forecast skill horizon, defined as the lead time at which a climatological distribution is as skilful as the forecast ensemble, Buizza and Leutbecher (2015) found that the forecast skill horizon extends beyond 2 weeks. For instantaneous, grid-point fields, such as Z500 over the Northern Hemisphere (NH) , the skill horizon is between 16 and 23 days. The authors note that forecast skill depends on the spatial and temporal scale of the field, the variable, the area, and the season. In the current work, we have used the 15-day ECMWF ensemble forecasts initialized both 10 and 5 days prior to GBE onset. Model reliability decreases, as expected, at longer forecast lead times; however, the 10-day lead times are well within the forecast skill horizon of the ECMWF model.

Matsueda (2009) assessed the forecast performance of nine TIGGE operational NWP centres, based on an examination of predictions of blocking frequency during three winters. Many of the models demonstrated reasonable skill in the forecasting of blocking; however the skill was lower in relation to the frequency of Greenland blocking during DJF of 2006/07 even at lead times of 5 days, and the performance of the ECMWF model was similar to that of the two other models reviewed for that winter (Matsueda, 2009). The ECMWF ensemble prediction system, which contributes to the TIGGE project, has been shown to be more skilful than the deterministic control forecasts at all forecast lead times, both short range and medium range, despite a slight under-forecasting bias (Pelly and Hoskins, 2003b); however, this study evaluated only Euro-Atlantic and Pacific sector blocking. Ferranti *et al.* (2015) assessed the flow-dependent skill of the ECMWF ensemble for five cold seasons, and found that forecasts initiated in the negative phase of the NAO were most skilful (Frame *et al.*, 2013). Inter-model comparisons suggest that the ECMWF model is at least as skilful as other models in predicting NAO-related jet regimes (e.g. Frame *et al.*, 2011). Studies by Hurrell *et al.* (2003) and Vitart *et al.* (2014) of ECMWF ensemble forecast skill showed improvements over time in forecasts of the NAO, up to about forecast day 13, and also in the prediction of sudden stratospheric warmings, illustrating the ability to forecast some phenomena at lead times of several weeks.

2.2 | Circulation indices and Greenland blocking episodes

The two-dimensional blocking index (2D B index) of Masato *et al.* (2013a) is used, and calculated on ERA-I 500 hPa geopotential height (Z500) following Masato *et al.* (2013b). The integrals

$$\overline{Z_i^{\mathrm{n}}} = \frac{2}{\Delta\phi}\int_{\phi_0}^{\phi_0+\frac{\Delta\phi}{2}} Z_i \,\mathrm{d}\phi; \qquad \overline{Z_i^{\mathrm{s}}} = \frac{2}{\Delta\phi}\int_{\phi_0-\frac{\Delta\phi}{2}}^{\phi_0} Z_i \,\mathrm{d}\phi \quad (1)$$

are calculated at every longitude point, with the base latitude ϕ_0 varying within the band 40°–70°N, and $\Delta\phi = 30°$. The 2D B index is defined as

$$B_i = \overline{Z_i^{\mathrm{n}}} - \overline{Z_i^{\mathrm{s}}}, \quad (2)$$

with positive B therefore associated with a large-scale reversal of the meridional gradient of Z500. Positive local maxima of B are then tracked subject to both temporal and spatial constraints. These criteria identify blocking events of at least 5 days duration, that have significant zonal and meridional extent and are quasi-stationary (see Masato *et al.* (2013b) for the detailed methodology. Note that all grid points where B is positive and that are within a prescribed distance of the event maximum are labelled as 'blocked' in this study.)

A GBE is then defined following Woollings *et al.* (2008), using the sector approach favoured in many blocking studies. A region in the western North Atlantic bounded by 50–70°N, 20–90°W is chosen here (box in Figure 1), to encompass the main Atlantic Ocean blocking centre identified by Masato *et al.* (2013a) (their fig. 2) and to avoid including European blocking events. If at least one point in this region is an event maximum (as above) then a GBE is said to occur. Each observed event has been examined to verify that it is real and of interest. Onset days are defined as the first day of a GBE after 5 consecutive days where no episode occurs, and decay days similarly as the last day of a GBE before 5 days without a defined episode. Since the data are 6-hourly, the start time of the GBE is defined to occur at 0600 UTC on the day on which blocking is first identified in the chosen region,

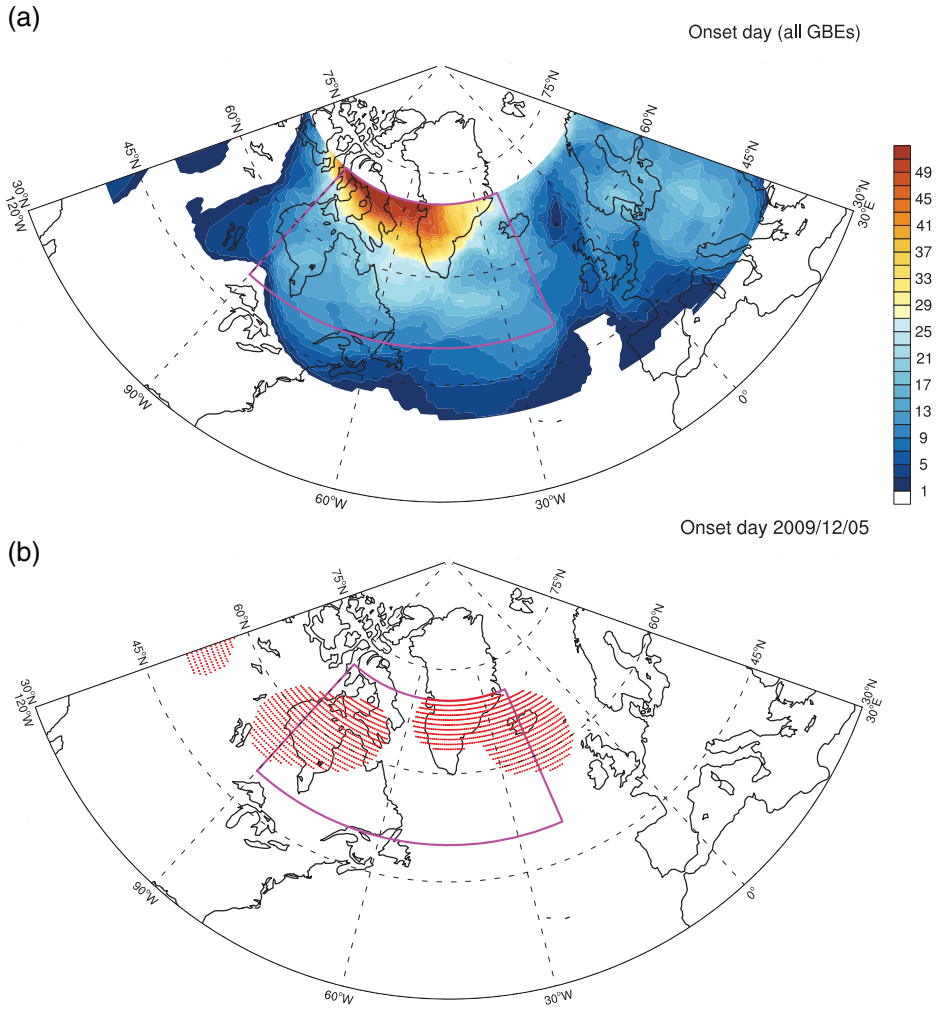

FIGURE 1 (a) Relative frequency of blocking on onset day for the 26 GBEs. All grid points with a positive 2D *B* index are counted and then summed and rescaled as a percentage of the total number of events. (b) indicates the grid points at which the 2D *B* index is positive (red dots) for the GBE case-study onset day of 5 December 2008. The magenta box indicates the region used to identify GBEs [Colour figure can be viewed at wileyonlinelibrary.com]

and ECMWF forecasts are initialized at 0000 UTC either 10 or 5 days prior to this start time. Onset day or 'day 0' is the period including the start time and the three subsequent 6-hourly time steps. The subsequent 24 h periods are termed days 1, 2, 3 and 4 subsequent to onset, respectively. Here we focus on the first few days of a GBE, and so for the forecast initialized 10 days prior (10-day forecast) to onset, the full 15-day ECMWF TIGGE forecast period is analysed, whereas for the forecast initialized 5 days prior (5-day forecast), only the first 10 days of data are used. For a GBE to be included in the defined set, the condition that at least one point in the defined Greenland box is identified as an event maximum must be met for *all* time steps during the last three days of the GBE (days 2–4 after first identification of a GBE). These criteria result in a total of approximately 162 GBE days out of a possible 812 DJF days, or about 20%, and 26 onset days and 24 decay days defined according to Woollings *et al.* (2008). A total of 42 instances of Greenland blocking are identified in the period if the criteria relating to onset days is relaxed.

The daily NAO index was obtained from the NOAA National Weather Service Climate Prediction Center (http://www.cpc.ncep.noaa.gov). The daily Madden–Julian Oscillation (MJO) index was sourced from the Australian Bureau of Meteorology (http://www.bom.gov.au) (both urls accessed 21 August 2018).

2.3 | Ensemble sensitivity analysis

Ancell and Hakim (2007) proposed an alternative, less computationally intensive, approach to adjoint-based sensitivity analysis by using the information contained in probabilistic forecast ensembles. The perturbed initial conditions and forecast fields of the ensemble are used to calculate a linear statistical relationship between a forecast metric and some precursor condition. Hakim and Torn (2008) first applied the method to an extratropical cyclone, confirming the influence of upper-level disturbances on surface cyclones as well as suggesting relationships to a surface cold front and a subtropical jet. Other applications include the climatological forecast sensitivity and the impact of observations on sea

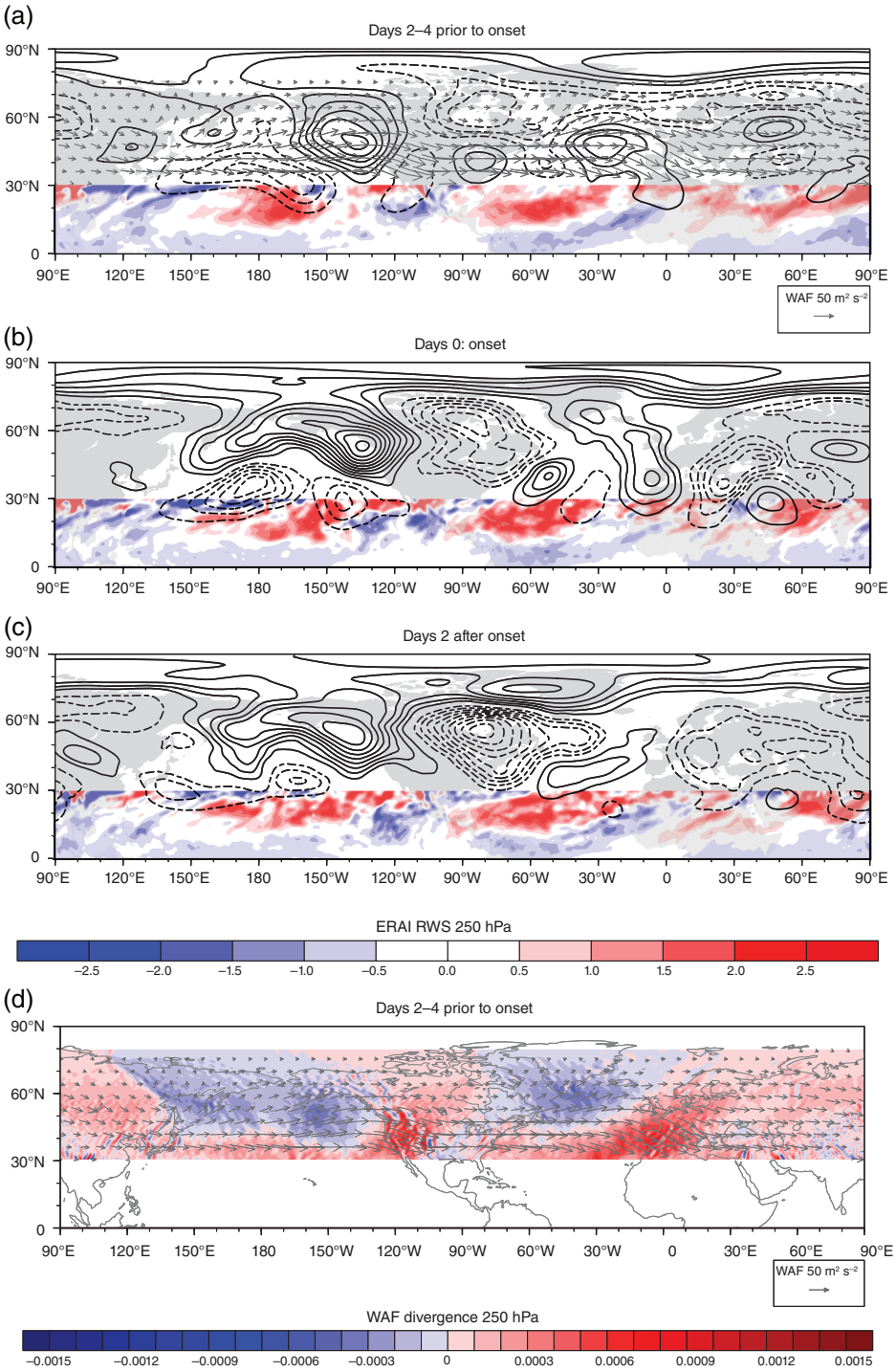

FIGURE 2 Composite of ERA-I 500 hPa geopotential height anomalies (a) averaged from 2 to 4 days prior to onset, (b) day 0; onset, and (c) day 2 after onset (black contours drawn every 10 gpm; zero contour omitted). Rossby wave source (RWS) at 250 hPa from 0–30°N is shown as colour shading (10^{-11} s^{-2}). (d) Composite of Rossby wave activity flux (WAF) divergence at 250 hPa averaged from 2 to 4 days prior to onset (colour shading). Vectors in (a) and (d) show the Rossby WAF at 250 hPa (m^2s^{-2}; a reference vector is at bottom right) [Colour figure can be viewed at wileyonlinelibrary.com]

level pressure and precipitation over western Washington State (Torn and Hakim, 2008), and a study of the dynamical processes responsible for the eastward track of hurricane *Sandy* in 2012 (Torn *et al.*, 2015). Such studies highlight the application of the sensitivity analysis method to targeted observation strategies and improved design of routine observation networks. Exploring ensemble sensitivities of the real atmosphere, Garcies and Homar (2009) applied the method to a set of clusters of Mediterranean intense cyclones, with the homogeneous classes in each cluster enabling the definition of relevant mean fields and hence the ensemble of perturbations required for sensitivity analysis. The difference in intensity between clusters of east and west North Atlantic extratropical cyclones in ERA-I data was similarly explored by Dacre and Gray (2015), using ensemble sensitivity to assess a variety of factors controlling cyclone development. Magnusson (2017)

used ensemble sensitivity analysis as one of a combination of methods to investigate three cases of extreme forecast errors or 'busts', using the ECMWF ensemble. Using the 6-day forecast error in 500 hPa geopotential height as the forecast metric, this study combined manual error tracking backward in time with sensitivity to 200 or 500 hPa geopotential height to identify probable source regions for the forecast error.

To calculate the sensitivity of GBEs to precursor fields, we follow the method outlined in Dacre and Gray (2015). The response function J is defined as the area-weighted average of the 2D B index of Masato *et al.* (2013b) within a box of 20° latitude × 20° longitude centred on the average position of the event maximum for days 2–4 after observed onset of the GBE. A linear regression is then calculated between the value of the response function J and the perturbation value x for all ensemble members k and at all grid points (i,j) of a precursor field from the ensemble mean value of that field. This yields a regression coefficient for the slope of

$$m_{ij} = \left(\frac{\partial J}{\partial x}\right)_{ij} = \frac{cov\left(J^k, x_{ij}^k\right)}{var\left(x_{ij}^k\right)}. \quad (3)$$

A correction factor is applied in order to control the weighting given to the calculated sensitivity at gridpoints where the regression has a poor correlation coefficient:

$$\alpha_{ij} = \begin{cases} 1 & \text{if } r_{ij}^2 \geq r_{\min}^2, \\ \frac{r_{ij}^2}{r_{\min}^2} & \text{if } r_{ij}^2 < r_{\min}^2. \end{cases} \quad (4)$$

The value of $r_{\min}^2$ is set to 0.076 here (using the t-statistic), such that gridpoints where the correlation is significant at the 95% level will remain uncorrected (i.e. $\alpha_{ij} = 1$).

As the variance of the precursor fields is climatologically lower at lower latitudes, the calculation includes a factor to account for the spatial variability of the variance of x_{ij}. Multiplication by the standard deviation σ_{ij} of the precursor field further results in the units of S being the same as those of the response function J, allowing the direct comparison of the sensitivity to a range of different precursors: the sensitivity can then be interpreted as the change in J associated with an increase in the precursor field by one standard deviation at that gridpoint.

The sensitivity S_{ij} is thus given by

$$S_{ij} = m_{ij}\alpha_{ij}\sigma_{ij}. \quad (5)$$

Typically we evaluate the sensitivity S of GBEs at a later date to the value of x at some previous time. Then positive/negative values of S_{ij} indicate that higher/lower values of x_{ij} at earlier times correspond to increased Greenland blocking shortly after GBE onset. The calculated sensitivity indicates a mathematical association between the response function and the precursor field, and thus is termed a *sensitivity* of the response to the precursor. However, the interpretation of the sensitivity relies on the postulation of a reasonable dynamical mechanism for the association, as well as the ensemble of forecasts exhibiting a spread of values in the precursor field in a particular region (Dacre and Gray, 2015). Here sensitivity is calculated using the ECMWF 51-member ensemble of 15-day forecasts, initialized both 10 and 5 days prior to onset of a GBE.

3 | PRECURSORS TO HIGH-LATITUDE BLOCKING IN ERA-I

3.1 | Tropospheric precursors

The 2D B index of Masato *et al.* (2013a; 2013b) is calculated on ERA-I Z500 for DJF 2006–2015. The relative occurrence of blocking for the onset day of the 26 GBE events only is calculated by counting and then summing all gridpoints where the 2D B index is positive, and expressing this as a percentage of the total number of events (Figure 1a). The centre of blocking over Greenland aligns well with the region over the northwestern Atlantic, on the poleward side of the jet stream, identified in the climatology of Masato *et al.* (2013a, their figs. 3 and 4) and characterized by cyclonic wave breaking in that study. Note that there is a lower frequency of blocking over Europe in Figure 1a (25%), in contrast to Woollings *et al.* (2008) where a high mean sea level pressure anomaly over Scandinavia is seen in composites for 4–2 days prior to onset of GBEs for winter in a 40-year reanalysis period (ERA-40).

Figure 2 (and Figure 3 top row, in polar stereographic form) shows the composite Z500 anomalies (from the mean Z500 for DJF 2006–2015) for the 26 identified GBE onset days. These show an anticyclonic feature north of Europe in the period before Greenland blocking, but this is further poleward than the anomalies typically associated with European blocking. The composite for days 2–4 prior to GBE onset (Figure 2a) shows a train of anomalies extending from the Pacific, across North America, and into the Atlantic. The major features are an area of anomalously low geopotential height over the central Pacific, a high over the Gulf of Alaska, lows over southwestern and northeastern North America, and a high over eastern North America, a low over the northwestern Atlantic and Greenland, and a high over the eastern Atlantic. This compares well with fig. 14 (top) of Woollings *et al.* (2008), which shows the composite 250 hPa streamfunction anomalies averaged over 2–4 days prior to 110 GBE onsets in ERA-40 data. The Rossby wave activity flux (WAF) at 250 hPa according to Takaya and Nakamura (2001) is shown by the vectors superimposed on the Z500 anomalies in Figure 2a. An extension of the Eliassen–Palm flux (Andrews and McIntyre, 1976), the WAF is parallel to the local Rossby wave group velocity and thus indicates the direction of the wave ray paths. The WAF indicates the Rossby wave train extending from the Pacific, over North America, and into the Atlantic. The flux converges into the amplifying ridge over

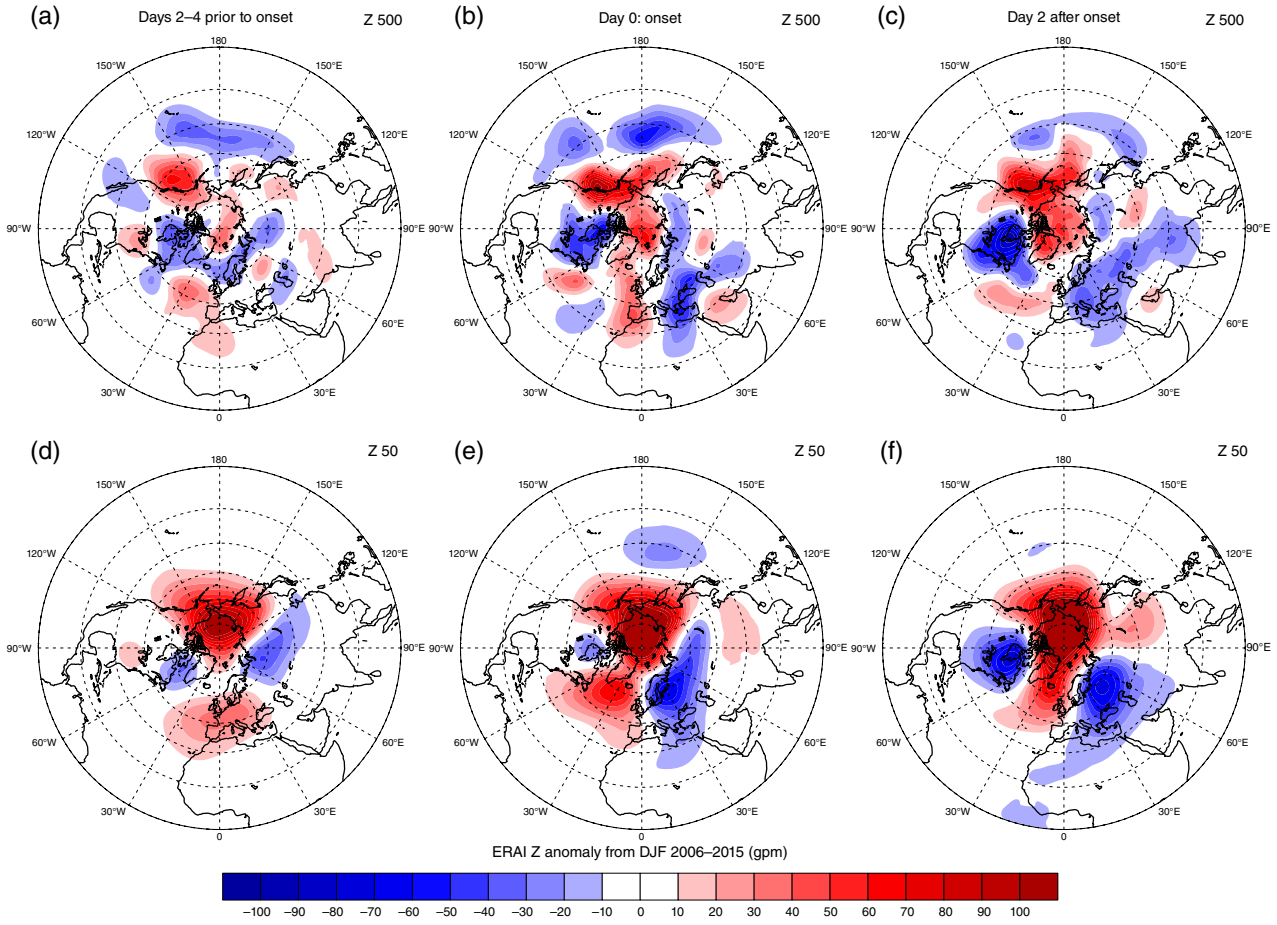

FIGURE 3 Composite of ERA-I geopotential height anomalies at (a, b, c) 500,hPa and (d, e, f) 50 hPa for (a, d) averages 2 to 4 days prior to GBE onset, (b, e) day 0 (onset), and (c, f) day 2 after onset [Colour figure can be viewed at wileyonlinelibrary.com]

Greenland and is divergent upstream (Figure 2d). As noted in Takaya and Nakamura (2001) and Nakamura and Anderson (1997), the convergence of WAF associated with an incoming stationary Rossby wave train can be of importance for blocking formation and may provide insight into the underlying dynamics. The colour shading in Figure 2a–c shows the Rossby wave source (RWS) in the Tropics, using the formulation by Sardeshmukh and Hoskins (1988) in which the RWS is defined as $-\nabla\cdot\left(v_\chi\,\xi\right)$, where v_χ is the divergent component of the horizontal velocity field and ξ is the absolute vorticity. While this plot shows the potential influence of the tropical Pacific via a Rossby wave train, this is not conclusive, and motivates the use of ensemble sensitivity analysis to determine whether Greenland blocking at some later time depends on the tropical Pacific at an earlier time. By onset day 0 (Figure 2b), the Z500 anomalies over the Pacific have intensified, as has the low over North America, while the high over the eastern Atlantic now extends to Greenland. A large area of anomalously low Z500 height extends across most of western Europe.

3.2 | Stratospheric precursors

The NH stratospheric polar vortex can be disrupted by propagating and breaking planetary waves from the troposphere, leading to disturbance and deceleration of the usual westerly flow and an associated dramatic warming of the polar stratosphere. Major sudden stratospheric warmings (SSWs), in which the polar vortex reverses direction, occur with a frequency of about six events per decade, and have significant impacts on the evolution of surface weather on time-scales of days to weeks (Baldwin and Dunkerton, 2001; Butler *et al.*, 2017). SSWs are often followed by an equatorward shift in the storm track, projecting onto the spatial pattern of the negative NAO phase. SSWs are classified into two types based on the characteristics of the disturbance of the reservoir of high potential vorticity (PV) in the polar stratosphere: displacement events and splitting events. Precursor wave activity is important for both types of SSWs, while anomalously strong zonal flow appears to be important only for vortex splits (Charlton and Polvani, 2007).

The rarity of stratospheric extreme events and the variability in blocking activity make it difficult to obtain statistically robust correlations between SSWs and blocking (Davini *et al.*, 2014). The interaction between the troposphere and stratosphere, and between tropospheric blocking and stratospheric SSWs, may be a two-way process (Martius *et al.*, 2009). An atmospheric block may trigger vertically propagating Rossby waves, disrupting the polar vortex and triggering

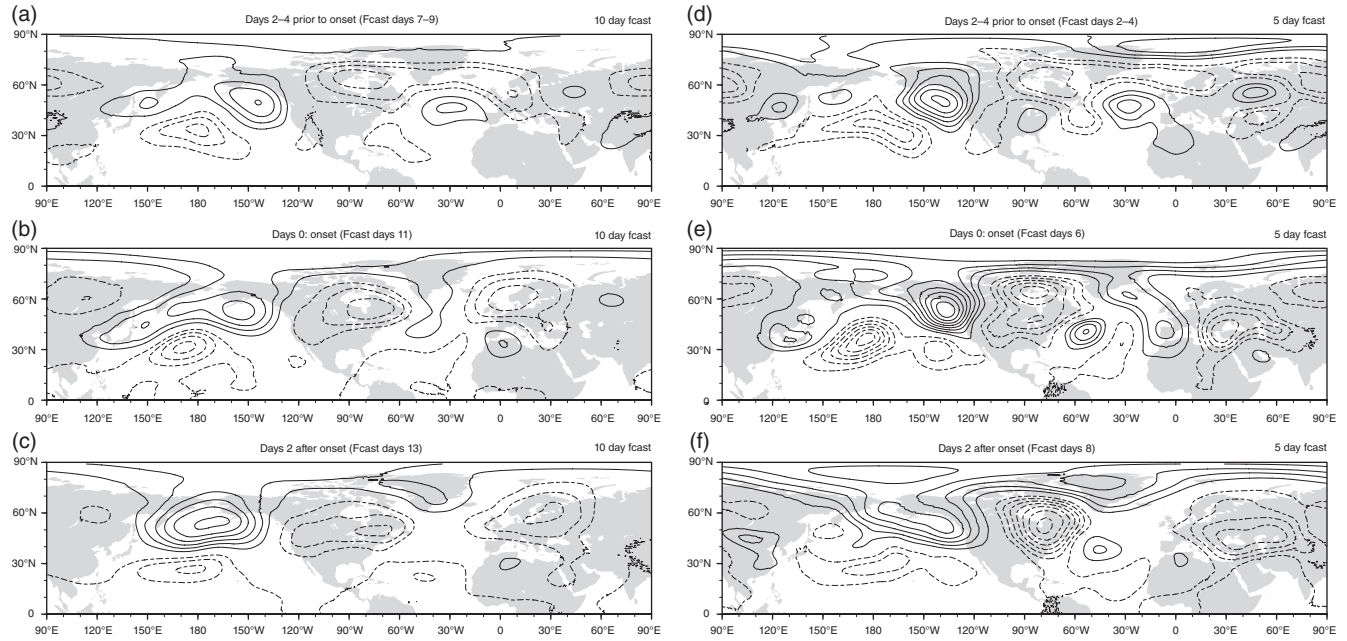

FIGURE 4 Composite of ECMWF ensemble mean 500 hPa geopotential height anomalies for (a, d) averaged from 2 to 4 days prior to onset, (b, e) day 0 (onset), and (c, f) day 2 after onset, for the forecasts initialized (a–c) 10 days and (d–f) 5 days prior to GBE onset

a SSW, although the majority of blocks are not followed by SSW events and the upward propagation of planetary waves into the stratosphere is strongly dependent on the geographical location of the blocking anticyclone (O'Neill and Taylor, 1979; Martius *et al.*, 2009; Castanheira and Barriopedro, 2010; Woollings *et al.*, 2010; Nishii *et al.*, 2011). The subsequent perturbed stratospheric flow may contribute to persistence of the block (Woollings *et al.*, 2010; Nishii *et al.*, 2011). The bottom-up precursor process associated with atmospheric blocking is comparatively rapid and therefore has implications for NWP, whereas the longer top-down influence of the SSW on surface weather evolution is important for extended-range and seasonal forecasts (e.g. Baldwin *et al.*, 2003; Mukougawa and Hirooka, 2004).

The stratospheric anomalies resulting from disturbances generated by vertically propagating waves from the troposphere can in turn descend to the surface on time-scales of weeks. As a result, storm tracks may shift and blocking frequencies at high latitudes may change (Baldwin and Dunkerton, 2001; Thompson and Wallace, 2001; Limpasuvan *et al.*, 2004). Mitchell *et al.* (2012) found that anomalies associated with a vortex splitting event have a greater surface effect than those related to a displacement event. However, Charlton and Polvani (2007) concluded that, while there was some difference in the spatial structures of the tropospheric impacts, the averaged tropospheric impact of the two types of events was similar.

Figure 3d,e,f shows the 50 hPa geopotential height (Z50) anomalies for the 26 GBEs. In the mean, the Aleutian anticyclone has strengthened. This high appears to be linked to the high in Z500 over the Gulf of Alaska (Figure 3a,b,c), but tilted towards the west with height. In general, the Z50 anomalies reflect a wave 2-type pattern, with positive anomalies over the pole and the northern sectors of the Pacific and Atlantic basins and negative anomalies over northeastern North America and northern Eurasia. As there are stratospheric anomalies in the period before blocking onset, as well as tropospheric precursors, ensemble sensitivity analysis will be performed using both Z50 and Z500 as precursor fields.

4 | PRECURSORS IN THE ECMWF TIGGE FORECAST ENSEMBLE

We now assess the representation of both tropospheric and stratospheric precursors in the ECMWF TIGGE forecast ensemble. All anomalies are taken as the difference between the ECMWF ensemble mean and the ERA-I mean for DJF 2006–2015 for the relevant variable. An alternative definition, using the ERA-I mean for all days covered by the 15-day ECMWF TIGGE forecast for all GBEs as the climatology, gives essentially similar anomalies (not shown).

4.1 | Tropospheric precursors

Figure 4 shows the composite ensemble mean Z500 anomalies for the ECMWF forecasts initialized 10 days (a–c) and 5 days (d–f) prior to GBE onset as defined above. Comparing the 10-day forecast composites to the ERA-I composites in Figure 2 shows that the major features are represented in the ensemble mean, although with reduced magnitude in some regions. The wave train extending from the Pacific over North America and into the Atlantic 2–4 days prior to onset is evident in Figure 4a, although the positive anomaly over the eastern coast of North America is absent. The similarities to the ERA-I composites continue for the day of onset and 2 days

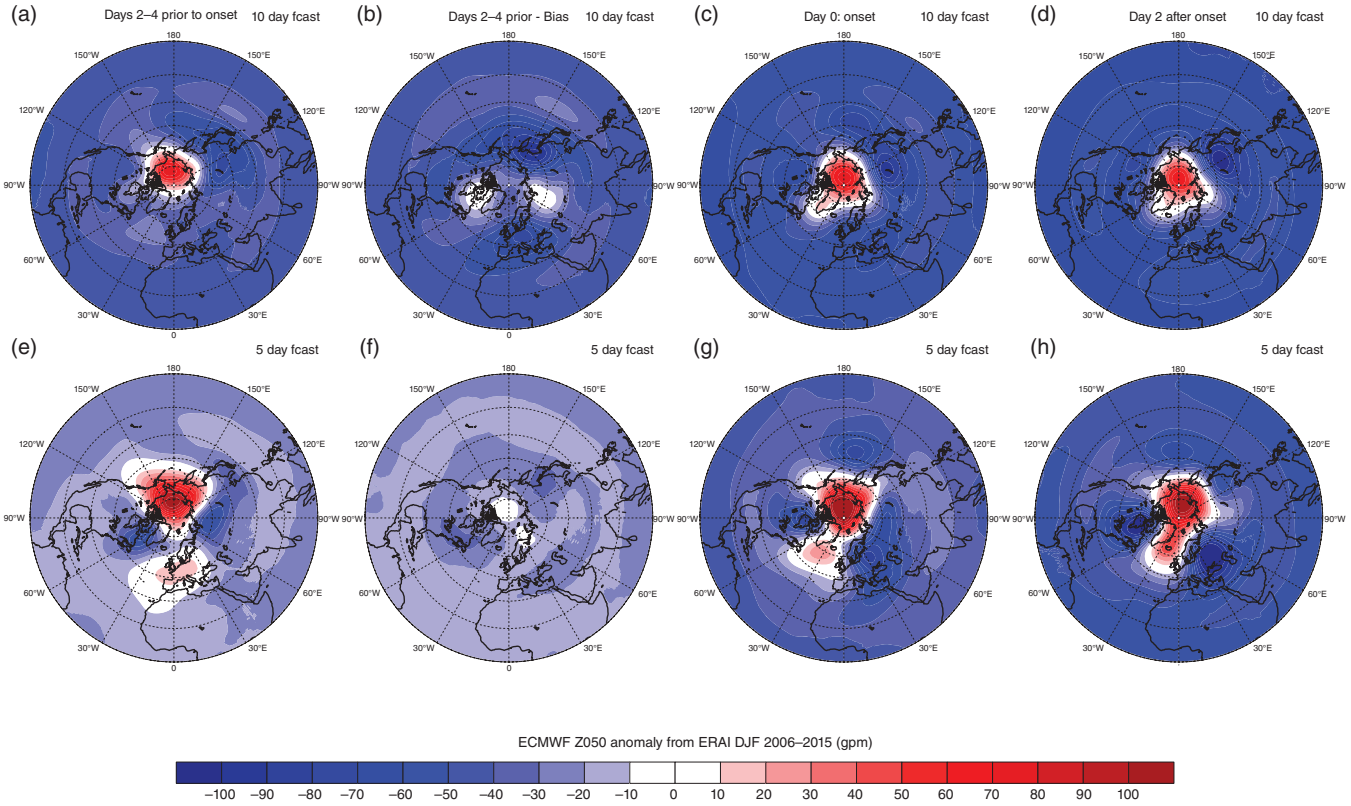

FIGURE 5 (a, c, d) and (e, g, h) are as Figures 3 and 4, but for the ECMWF forecast ensemble means at 50 hPa, for the forecasts initialized 10 days and 5 days respectively prior to onset. (b, f) show the difference between the ensemble means and the composite ERA-I anomalies for days 2–4 prior to onset, and illustrate the cold stratospheric bias in the model [Colour figure can be viewed at wileyonlinelibrary.com]

subsequently (Figure 4b,c). The intrinsic uncertainty in the atmospheric state results in a spread in the model ensemble for the 10-day forecast, with some members predicting the wave (and potentially other) precursors to blocking and other members predicting quite different evolutions in the flow. The differences between ensemble members that predict the precursor field and those that do not form the basis for the ensemble sensitivity analysis. The composites for the 5-day forecast (Figure 4d–f) more closely resemble the reanalysis, as would be expected at the shorter forecast lead time, with a correspondingly smaller spread in the ensemble. These results indicate that the observed precursor in Z500 does reflect a predictable signal leading to GBE onset, and that the ECMWF forecast model can capture this predictable signal even at lead times of up to 10 days in some cases.

4.2 | Stratospheric precursors

Figure 5 shows the composite ensemble mean Z50 anomalies for the ECMWF 10-day (a–d) and 5-day (e–h) forecasts. For the 10-day forecasts (a, c, d) , the anomalies in the Tropics and midlatitudes are appreciably more negative than in the ERA-I composite (Figure 3d–f), and the positive anomalies are restricted to the polar region; the highs over the Aleutians and the northern Atlantic basin are absent. Similar differences are evident in the 5-day forecast (Figure 5e,g,h), although the positive anomalies over the polar region extend slightly further from the pole. The wave 2 signature seen in the reanalysis composites is evident in the 5-day forecast panels, but is not clear in those for the 10-day forecast. In general, the forecast composites show an anomalously cold stratosphere. Removing the ERA-I composite anomalies (Figure 3a,d) from the composite ensemble mean (Figure 5a,e) for days 2–4 prior to onset reveals that the cold stratospheric bias is widespread and exhibits no particular structure (Figure 5b,f). The bias develops very early in the forecast period and spreads throughout the NH by the end of the first day of both forecasts (not shown). These results indicate that the bottom-up process, whereby vertically propagating Rossby waves from the troposphere disrupt the polar vortex in the stratosphere, may not be well captured by the ECMWF forecast model.

SSWs are routinely identified using the daily-mean zonal winds at 60°N and 10 hPa (Charlton and Polvani, 2007); however, no attempt has been made in this study to identify SSWs or to categorize them as either vortex-splitting or vortex-displacement events, in either the reanalysis or forecast composites.

5 | A CASE-STUDY OF A GREENLAND BLOCKING EPISODE

To illustrate the composite results above, a case-study of a GBE is briefly examined. The winter of 2010 was

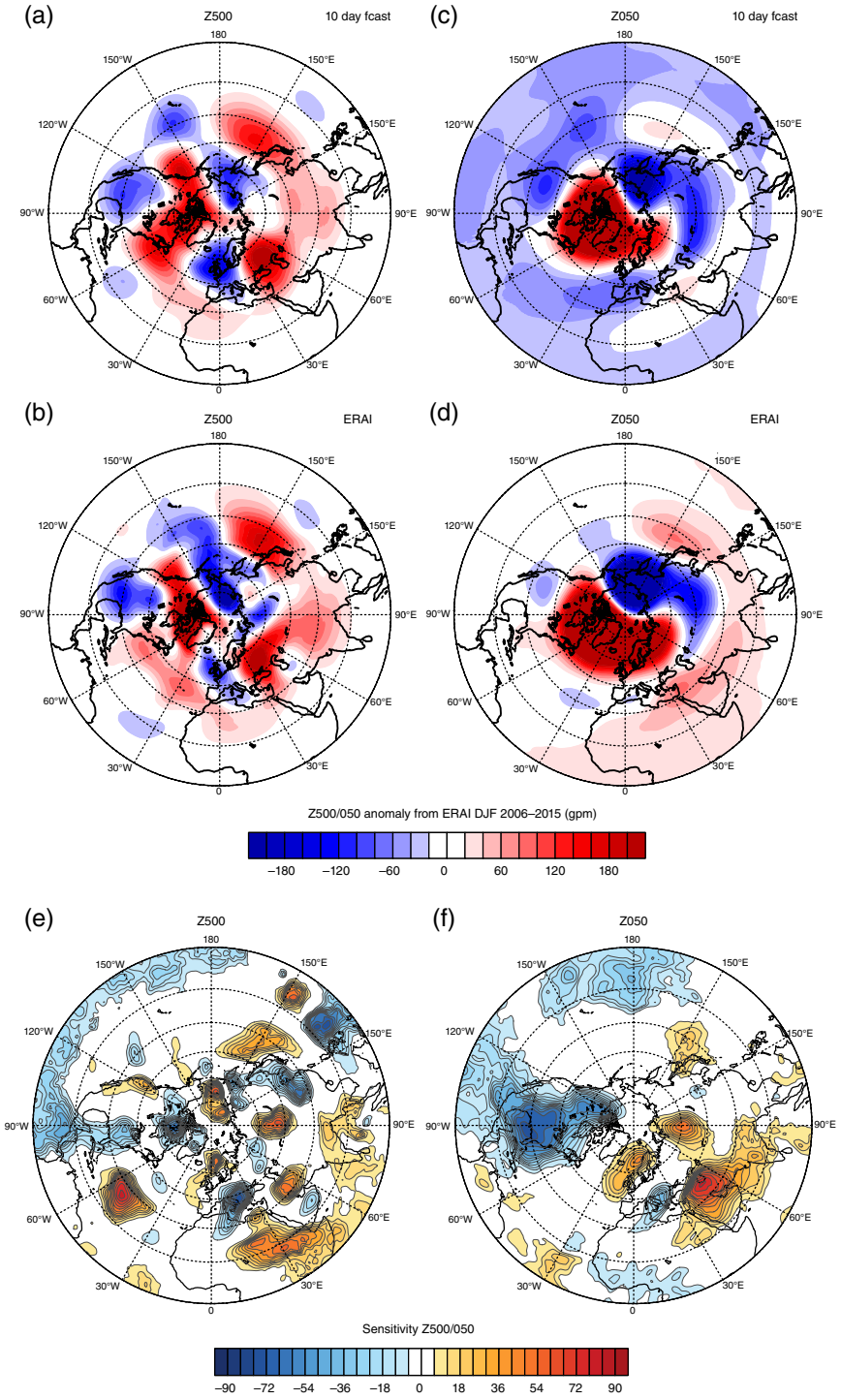

FIGURE 6 For GBE onset 5 December 2009 for (a, c, e) Z500 and (b, d, f) Z50. Mean anomaly (gpm) from ERA-I mean DJF 2006–2015 for days 2–4 prior to GBE onset for: (a, c) ECMWF 10-day forecast ensemble mean, and (b, d) ERA-I reanalysis. (e, f) show sensitivity of mean 2D *B* index over Greenland averaged over days 2 to 4 after onset, to Z500/50 respectively at day 2 prior to onset (forecast day 9). Units are those of the 2D *B* index, i.e. geopotential height (gpm) per standard deviation of the precursor field [Colour figure can be viewed at wileyonlinelibrary.com]

characterized by a negative phase of the NAO, a southerly jet regime, and weak flow associated with episodes of strong cyclonic Rossby wave breaking and blocking over Greenland. This winter also marks the beginning of one of the ten most significant droughts in lowland England in the past 100 years. Drought conditions developed as a result of persistent blocking during 2010, with rainfall deficiencies concentrated in spring, autumn and winter. The drought was dramatically terminated in the late spring and summer of 2012 by record rainfall, with the April–June period the wettest in a historical series extending back to 1766 (Marsh *et al.*, 2013).

The GBE selected for this case-study occurred during the winter of 2010, with onset on 5 December and decay occurring on 11 December 2009 respectively (with onset and decay as defined in section 2.2). A map of the positive 2D *B* index at GBE onset for this event is shown in Figure 1b,

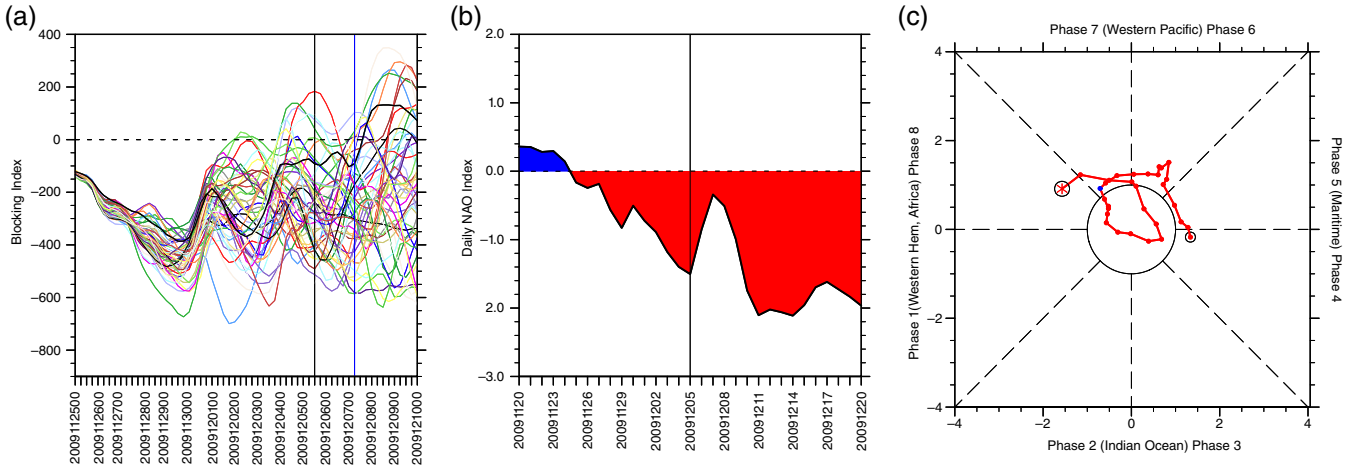

FIGURE 7 For GBE onset 5 December 2009. (a) 2D *B* index for ECMWF ensemble forecasts initialized on 25 November 2009. Randomly coloured lines indicate individual ensemble members, and the thick black line indicates the observed ERA-I *B* index. The black vertical line marks the (observed) GBE onset date, and blue vertical line the start of days 2 to 4 after blocking onset, over which the mean blocking index used in the sensitivity calculations is averaged. (b) Daily NAO index and (c) MJO index from 15 days prior to 15 days subsequent to GBE onset. For the MJO phase plot, a red dot in an open black circle denotes the start time, red dots denote the daily index, a blue dot marks GBE onset, and a red asterisk in an open black circle denotes the end time [Colour figure can be viewed at wileyonlinelibrary.com]

with blocking at high latitudes over Greenland and Hudson Bay in northeastern Canada. (Note that the centre of blocking over Hudson Bay does not satisfy the spatial and temporal constraints of the blocking methodology, and so does not constitute a blocking event.)

A comparison of the Z500 anomalies averaged over days 2–4 prior to GBE onset (forecast days 7–9) in the forecast versus the reanalysis is shown in Figure 6a,b. The ensemble mean for the ECMWF 10-day forecast (a) is in good agreement with the ERA-I reanalysis anomalies (b), with a pattern of alternating ridges and troughs extending from the western Pacific across North America to the Atlantic basin. As for the ensemble sensitivity (Figure 6e) the regions of negative sensitivity over the southeastern part of North America and positive sensitivity over the Atlantic Ocean to the east are adjacent to the trough over southern North America and ridge over the Atlantic to the east seen in the Z500 anomalies (Figure 6a,b). The alignment of these sensitivities with respect to the wave precursor suggests that for this case the blocking was sensitive to the phase propagation of the precursor. There is an extensive region of negative ensemble sensitivity at low latitudes over the Pacific Ocean. (Note that the contour intervals in Figure 6e,f are different from those used for the composite sensitivity analysis below, and that the sensitivities seen in the case-study panels are larger in magnitude.)

For the stratospheric precursor, the ensemble mean Z50 anomalies (Figure 6c) are in broad agreement with the reanalysis (Figure 6d) at high latitudes, but the midlatitudes and equatorial stratosphere again show the cold stratospheric bias in the ECMWF ensemble model. The stratospheric anomalies in this case resemble the pattern seen during polar vortex displacements; however, no attempt has been made to classify these event types, as discussed previously. The ensemble sensitivities may reflect the cold stratospheric bias outside the high latitudes, as mentioned above. For this GBE (Figure 6f) there is a large region of negative sensitivity over North America, adjacent to a small region of negative Z50 anomalies seen in the reanalysis (Figure 6d); positive sensitivity is evident at high latitudes between Greenland and Scandinavia and over northern Asia, where positive Z50 anomalies are apparent. As for the tropospheric sensitivity, the alignment of the stratospheric sensitivities with respect to the wave precursor suggests a sensitivity to the phase propagation of the precursor in this case.

Figure 7a illustrates the timeline for the ECMWF 10-day forecast for this GBE: the ensemble is initialized 10 days prior to GBE onset, and the area mean 2D *B* index is calculated at all timesteps of the 15-day forecast run. As discussed in section 2.3, the increasing spread in the 2D *B* index with time across the ensemble can be clearly seen in this plot. The aim of the sensitivity analysis is to utilize that spread to relate the response function to a precursor field at an earlier forecast time. Here we examine the assocation between the spread in the 2D *B* index averaged over days 2–4 after blocking onset, and the chosen precursor atmospheric variables at some earlier forecast time, and propose reasonable dynamical mechanisms for such an assocation. For this GBE the ensemble of forecasts is able to capture the observed outcome at some later time, with the reanalysis 2D *B* index contained within the ensemble spread. The ensemble 2D *B* index diverges from around forecast day 4 onwards, although the general trend in the index is apparent until around forecast day 6.

The GBE case-study occurred during a period of persistently negative NAO which lasted from early 2009 until late 2011, and is in fact the most persistently negative period from 1979 onwards (not shown). Figure 7b shows the daily NAO index for a period from 15 days prior to 15 days subsequent

to GBE onset for this case. The NAO becomes negative some 12 days prior to onset and this state persists for the entire period considered. It should be noted that the development of the NAO index does not show a consistent pattern across all GBEs (not shown).

As discussed further in section 6.1, Cassou (2008) found that phase 6 of the MJO may contribute to the formation of NAO–. Figure 7c shows the evolution of the phase of the MJO in phase space, for the same period as the NAO panels above, for the GBE examined here. Fifteen days prior to GBE onset, the MJO is in phases 4–5, characterised by enhanced convection over the Maritime Continent. The MJO then progresses through phase 6 to reach phase 7 by onset, with phases 6–7 characterized by enchanced convection over the Pacific. The MJO then becomes weak (the amplitude is within the inner circle of the phase space) before returning to larger amplitudes in phase 7 and 8. Note that not all GBEs show a progression through MJO phase 6 prior to the start of blocking and, of those that do, the amplitude is frequently weak (not shown). The results relating to the MJO and NAO indices should also be interpreted in the light of the particular indices used; other methods of deriving these indices may produce different results. However, this would require further exploration and is not within the scope of the present work.

6 | ENSEMBLE SENSITIVITY ANALYSIS USING ECMWF TIGGE FORECASTS

The ECMWF TIGGE forecast ensemble is used to calculate the sensitivity of GBEs to a variety of precursor fields, as outlined in section 2.3 above. Following from the examination of Z500 and Z50 precursors to GBEs discussed previously, these two fields are chosen as the precursor variables in the following analysis.

6.1 | Sensitivity of Greenland blocking episodes to 500 hPa geopotential height

The ensemble sensitivity of the area-mean 2D blocking index, calculated within a box of 20° latitude × 20° longitude centred on the average position of the event maximum for days 2–4 after observed onset of the GBE, to Z500 at all forecast lead times has been calculated as outlined previously. Figure 8a–c show the composite sensitivity at forecast days 7, 9 and 11 respectively (i.e. 4 days and 2 days prior to onset, and onset day) for the ECMWF forecast initialized 10 days prior to the first day of the 26 GBEs (results for all 42 instances of Greenland blocking are almost identical – not shown). The composite was formed by calculating the sensitivity fields separately for each event and then averaging. Positive/negative sensitivity values indicate that higher/lower Z500 heights in those regions will lead to increased blocking over Greenland (i.e. an increase in the blocking index) at the chosen time. The units of the sensitivity are those of the 2D blocking index, namely geopotential metres (gpm) per standard deviation of the precursor field.

At 4 and 2 days prior to onset of the GBEs (Figure 8a,b), the pattern of sensitivity is qualitatively similar to the pattern of Z500 precursors discussed above (Figure 4a,b). There are regions of positive sensitivity over the central Pacific basin at midlatitudes, over the Gulf of Alaska, and over eastern North America. Regions of negative sensitivity also extend across the Pacific Ocean at lower latitudes, including the central and eastern Pacific, as well as across the Atlantic at the latitudes of the eddy-driven jet. There are regions of sensitivity over much of the hemisphere. This does not, of course, necessarily imply causality, but it does highlight the globally connected nature of the dynamics in these periods.

Furthermore, there are indications that these signals endure as a consequence of the developing GBE. By onset day, over the Atlantic basin the pattern is a tripole of positive sensitivity over Greenland and the polar regions as well as over the Atlantic and West Africa at lower latitudes, with a band of negative sensitivity extending across the ocean basin at the latitudes of the eddy-driven jet. This tripole is consistent with a shift of the jet from higher to lower latitudes, with easterly wind anomalies near the polar regions and westerly anomalies in midlatitudes.

For the ECMWF forecast initialized 5 days prior to GBE onset, the magnitude of the sensitivities is slightly smaller, and the sensitivity to the tropical Pacific is not as marked at these shorter forecast lead times, though still apparent (Figure 9). In general, the regions of sensitivity are more widespread for the 10-day forecast, and more local to the precursor pattern for the 5-day forecast.

Given the widespread nature of the sensitivities on average, it is of interest to consider how many individual GBEs also show significant sensitivity over much of the hemisphere. Figure 10a–c show the percentage of GBEs with uncorrected (i.e. correction factor = 1) sensitivity, both positive and negative, to Z500 for the same forecast lead times as in Figure 8. Note that uncorrected sensitivity corresponds to sensitivity that is statistically significant at the 95% level in this context. This is done by counting the number of GBEs with uncorrected sensitivity at one or more gridpoints in each box of 30° longitude × 15° latitude indicated by the gridlines on the maps, and representing this number as a percentage of the total of 26 GBEs. A clear conclusion from this analysis is that the GBEs exhibit significant sensitivity to large regions of the NH, although these regions are not the same for all GBE events. For example, four days prior to onset (Figure 10a), between 50 and 80% of events have significant sensitivity in the tropical Pacific, and by 2 days prior to onset this pattern extends to the tropical region across the NH, although with slightly lower maximum values (Figure 10b). The results demonstrate the robustness of the sensitivities in regions where precursors to GBEs have been identified and where the sensitivities in Figure 8 are largest in value. A further result is

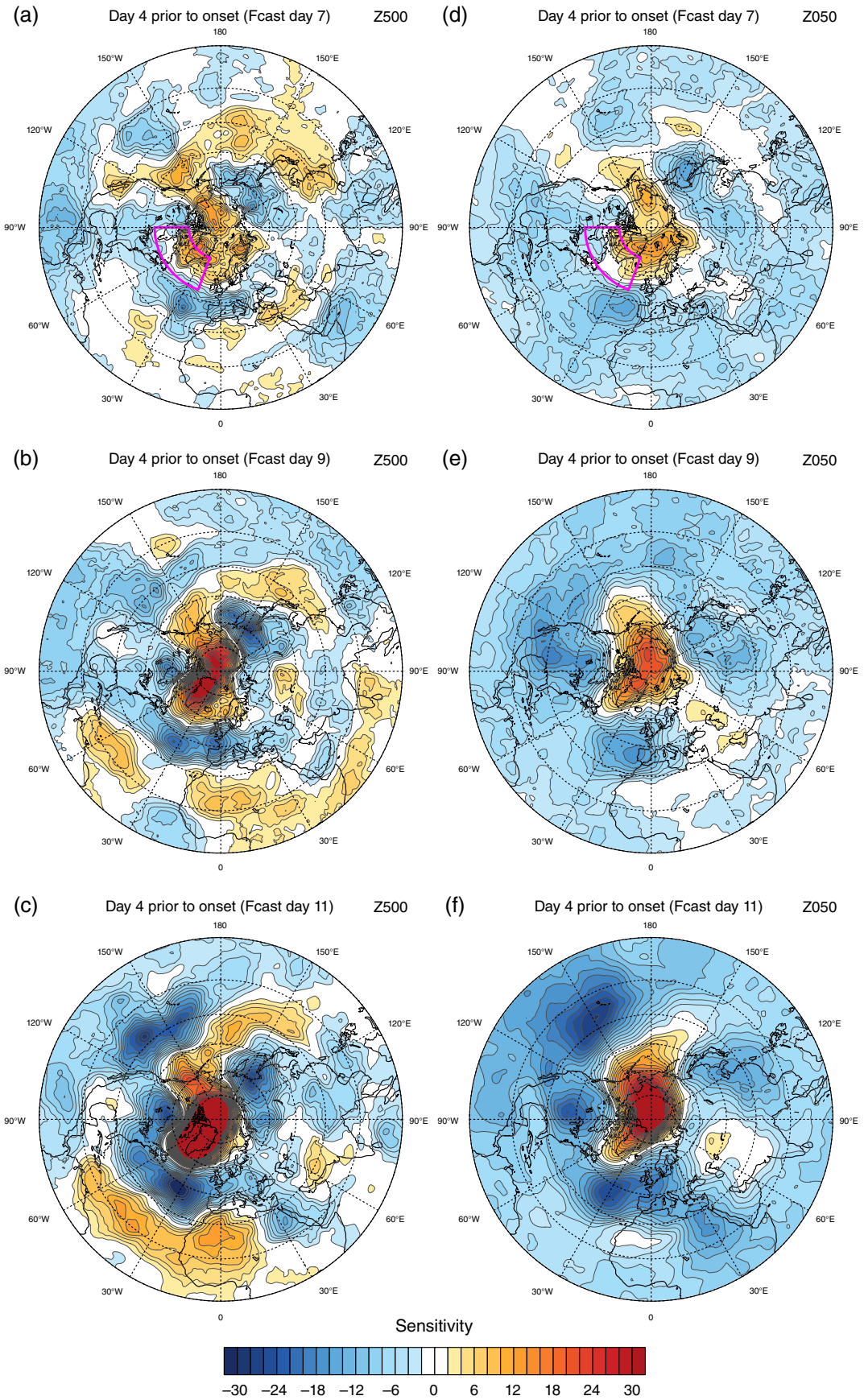

FIGURE 8 Ensemble mean sensitivity (colour shading) of mean 2D *B* index over Greenland (magenta box) averaged over days 2 to 4 after onset, to (a–c) Z500 and (d–f) Z50. For ECMWF forecasts initialized 10 days prior to onset, at (a, d) day 4 prior to onset (forecast day 7), (b, e) day 2 prior to onset (forecast day 9), and (c, f) day 0 (onset; forecast day 11). Units are those of the 2D *B* index, i.e. geopotential height (gpm) per standard deviation of the precursor field [Colour figure can be viewed at wileyonlinelibrary.com]

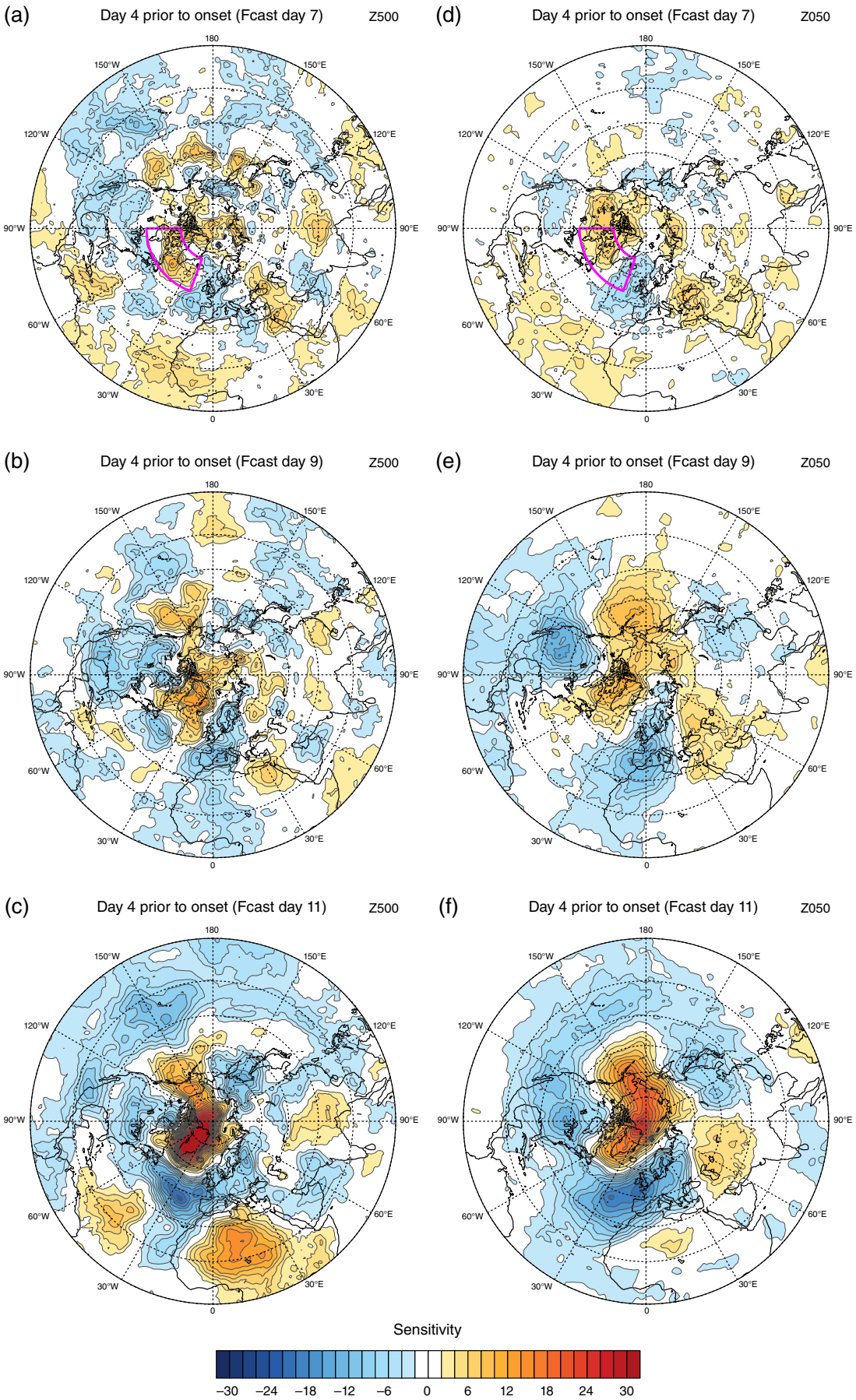

FIGURE 9 As Figure 8, but for ECMWF forecasts initialized 5 days prior to onset, at (a, d) day 4 prior to onset (forecast day 2), (b, e) day 2 prior to onset (forecast day 4), and (c, f) day 0 (onset; forecast day 6) [Colour figure can be viewed at wileyonlinelibrary.com]

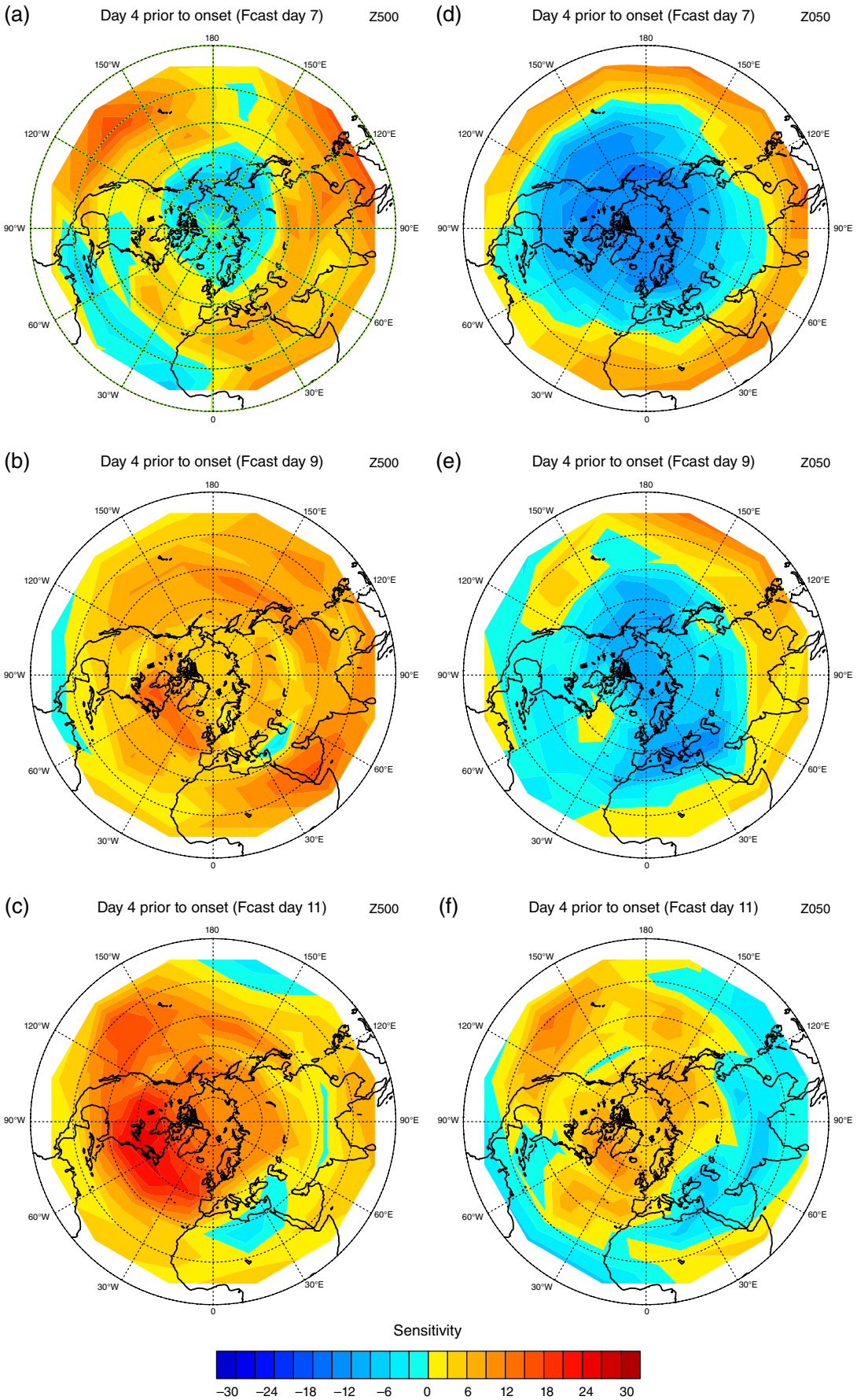

FIGURE 10 Percentage of the 26 GBEs with uncorrected sensitivity to (a–c) Z500 and (d–f) Z50 at one or more gridpoints in each box of 30° longitude × 15° latitude indicated by the gridlines, for ECMWF forecasts initialized 10 days prior to GBE onset at forecast lead times as in Figure 8 [Colour figure can be viewed at wileyonlinelibrary.com]

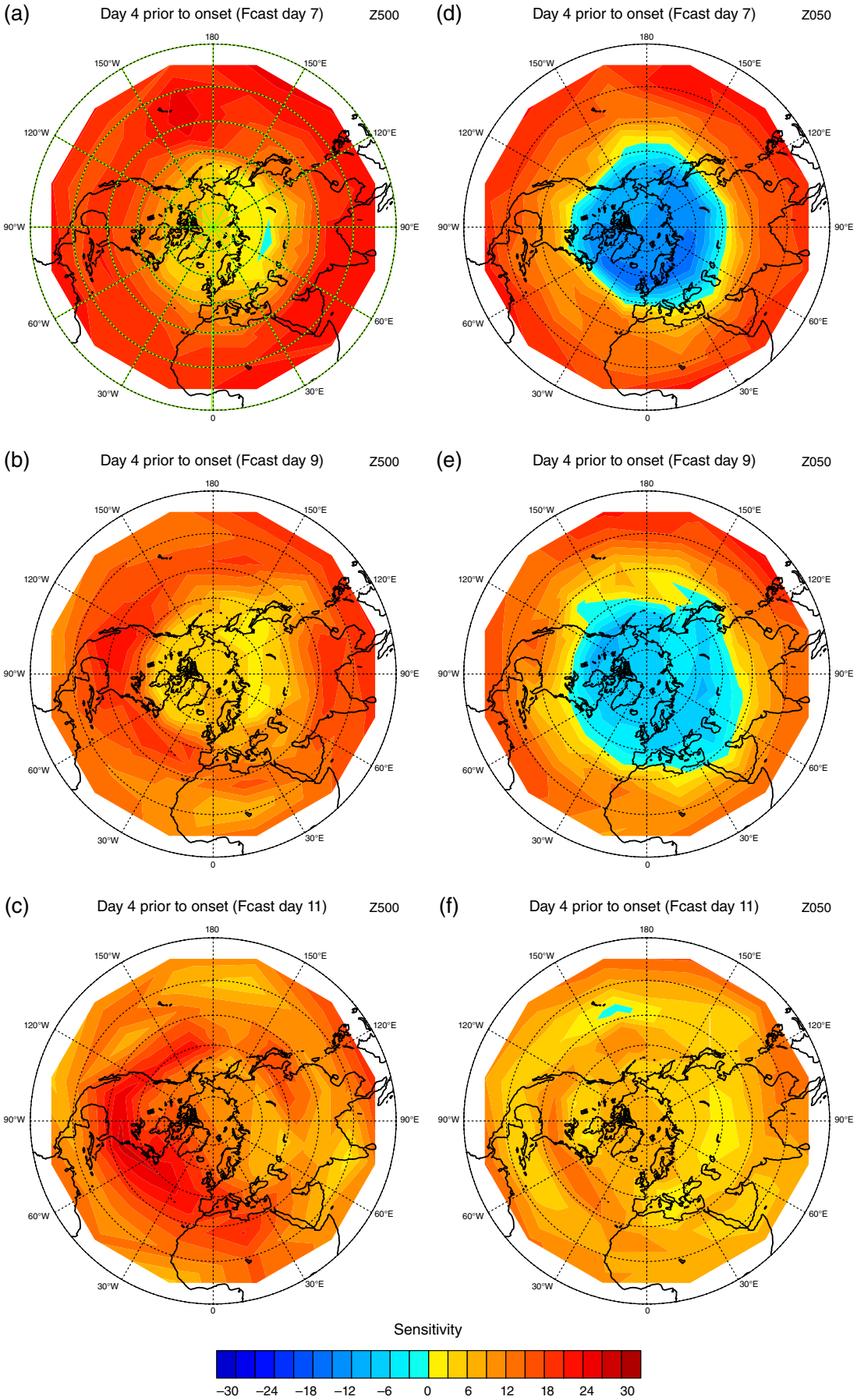

FIGURE 11 As Figure 10, but for ECMWF forecasts initialized 5 days prior to GBE onset at forecast lead times as in Figure 9 [Colour figure can be viewed at wileyonlinelibrary.com]

that the higher counts at lower latitudes in Figure 10a,b indicate that GBEs are more often sensitive to the tropical regions than to the Arctic, in agreement with Jung *et al.* (2014).

For the 5-day forecast (Figure 11), the proportion of GBEs with uncorrected sensitivity to Z500 in the Tropics 4 and 2 days prior to onset is between 50 and 90% across the NH. Hence, there are more significant sensitivities, although the actual sensitivity values are lower (Figure 9). The region where most events have significant sensitivity to Z500 is aligned with the precursor regions, where the forecast precursors closely resemble the observations. GBEs are again more often sensitive to the Tropics than to the polar regions at this shorter forecast lead time.

A simple 24 h difference (high-pass) filter is applied to the Z500 field (e.g. Wallace *et al.*, 1988) to examine the sensitivity of GBEs to the high- versus low-frequency components of the geopotential height field for the 10-day forecast only (Figure 12). The high-frequency component of the sensitivity (a–c) is cyclonic over the North Atlantic and particularly over the Gulf Stream. Woollings *et al.* (2008) found anomalously strong storm activity in transient eddy kinetic energy at the start of the Atlantic storm track before GBE onset (their fig. 6). The southward extent of this activity suggests that the eddies may advect warm air from the Subtropics to the poleward side of the jet. The sensitivity to the low-frequency component of Z500 (Figure 12d–f) is larger in magnitude than the high-frequency sensitivity, indicating that the spread in Greenland blocking is mostly due to the low-frequency dynamics, and there is evidence of a wave precursor in the tropical Pacific.

The Z500 sensitivity results suggest that the tropical east Pacific may be influencing the onset of GBEs. Cassou (2008) constructed lagged composites between the MJO, which is the dominant component of intra-seasonal variability in the tropical atmosphere, and the NAO. The MJO is characterized by eastwards displacement of enhanced precipitation with associated modifications to upper-level atmospheric circulation. This study identified phase 6 of the MJO as a precursor of the NAO– regime, suggesting that enhanced convection over the eastern Pacific in this phase is associated with upper-level divergence and hence a Rossby wave source, and compensating convergence at the entrance to and on the southern flank of the climatological jet stream. Rivière and Orlanski (2007) found that enhanced moisture upstream from the North Atlantic storm track, consistent with the anomalous upper-tropospheric circulation in phase 6 of the MJO, destabilizes the atmosphere and favours cyclonic wave breaking, and may contribute to formation of NAO–. Henderson *et al.* (2016) find that both Atlantic and European blocking frequencies are affected by the teleconnection patterns associated with some phases of the MJO, proposing both the resulting NAO variability and changing PNA patterns as precursors to blocking increase or decrease.

Furthermore, the region of negative sensitivity for the 5-day forecast over the northwest of North America at around 30–45°N, 120°W (Figure 9) corresponds to the 'Rockies trough' region of Rodwell *et al.* (2013) (their fig. 4a). This region of anomalously low Z500 is a robust feature of 584 European forecast 'busts' in all seasons from January 1989 to June 2010, and is apparently embedded in a Rossby wave train over the United States. While their study focuses on a different region, the dynamics of the large-scale flow are potentially similar to GBEs.

It is also of interest to note that forecast errors are not bound to the phase speed of Rossby waves, but may propagate at the wave group speed (e.g. Kelly *et al.* 2007). As a result, for example, initial condition errors over the Pacific may impact short-term (6-day) forecasts over Europe (Magnusson, 2017).

Woollings *et al.* (2008) found a large anticyclonic anomaly over Europe in the 250 hPa streamfunction averaged over 2–4 days prior to GBE onset (their fig. 14, top panel), consistent with suggestions that GBEs may often be preceded by atmospheric blocking over Europe. One proposed mechanism suggests that wave breaking in the diffluent region upstream of a European block shifts the blocking anticyclone westwards (Tyrlis and Hoskins, 2008; Woollings *et al.*, 2008; Sung *et al.*, 2011; Luo *et al.*, 2015). A second possible mechanism for upstream propagation of blocking is linear wave propagation, as discussed in the simple model of Luo *et al.* (2007). A positive anomaly is evident in the Z500 precursors in the ERA-I observations for the period examined here (Figures 2 and 3a–c), but it is a long way north, poleward of Scandinavia. There are significant sensitivities in this region (Figure 8a), though not in the majority of cases until 2 days prior to onset (Figure 10). This indicates that, while there is indeed some form of upstream influence, it is not obviously linked to European blocking in these events. Large areas of negative sensitivity are seen over the rest of Europe in the 10-day forecast composites (Figure 8a,b). Note that the statistical significance of the European block in Woollings *et al.* (2008) was low, with a single significant positive correlation for the block leading the GBE at a lag time of 2 days (their fig. 16).

6.2 | Sensitivity of Greenland blocking episodes to 50 hPa geopotential height

Figures 8d–f show the composite ensemble mean sensitivity of Greenland blocking to Z50 at forecast days 7, 9 and 11 respectively (i.e. 4 and 2 days prior to GBE onset, and onset day) for the 10-day forecast. As for Z500, there are large regions of negative sensitivity over the central Pacific basin at midlatitudes, over the eastern tropical Pacific, and over the North Atlantic Ocean in the vicinity of the storm track. Areas of positive sensitivity are largely confined to the polar region at high latitudes, and a small area over the Aleutians and over the Asian continent at around 60° E. The results for the 5-day forecast (Figure 9d–f) are similar, again with reduced magnitudes and less widespread negative sensitivity over the Pacific

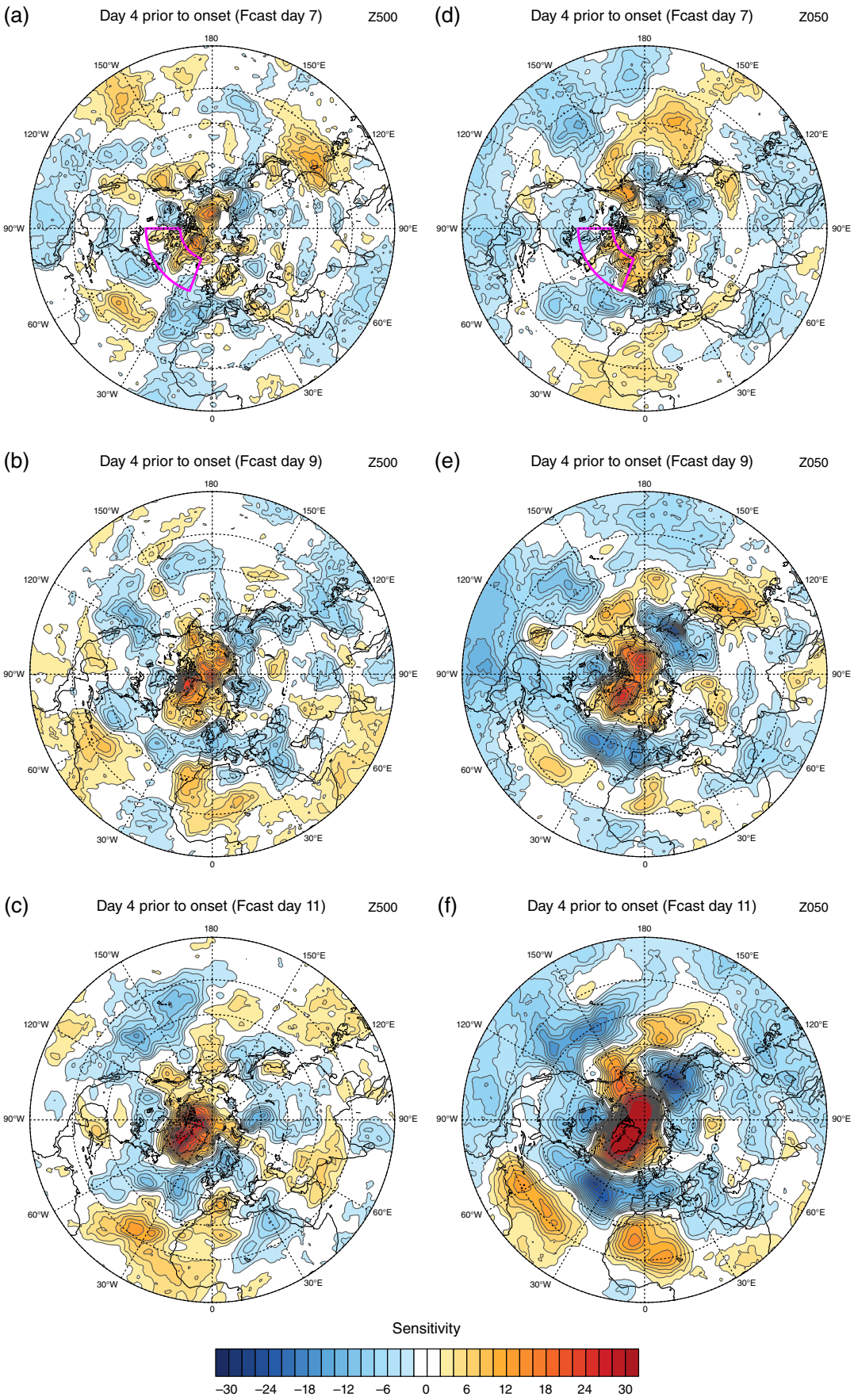

FIGURE 12 As Figure 8 for the 10-day forecasts, but for ensemble mean sensitivity to (a–c) high-frequency and (d–f) low-frequency components of Z500, separated using a simple 24 h difference filter [Colour figure can be viewed at wileyonlinelibrary.com]

Basin. A dipole pattern of positive sensitivities in the polar regions and negative over the Atlantic Basin is established by the time of GBE onset in both cases, as expected.

However, Figure 5b,f show a widespread cold stratospheric bias in the ECMWF forecasts, while the observations for Z50 in Figure 3d–f do not show precursors to GBEs at low latitudes. It therefore seems likely that the large regions of negative sensitivity seen in the 10-day forecast (Figure 8d–f) and the 5-day forecast (Figure 9e,f) represent the ensemble sensitivity to the stratospheric bias. Hence, the rate at which the stratospheric bias establishes might be related to the likelihood of Greenland blocking, although the cause and effect relationship here is not obvious.

The percentage of GBEs with uncorrected sensitivity to Z50 at one or more gridpoints in the boxes defined previously is shown in Figures 10d–f and 11d–f for the 10- and 5-day forecasts respectively. There are fewer GBEs with uncorrected sensitivities at higher latitudes than for the Z500 case, particularly for the 10-day forecast. The majority of GBEs show uncorrected sensitivities to lower latitudes for the forecast initialized 5 days prior to GBE onset. However, these results must be interpreted in the light of the probable sensitivity to the stratospheric bias as discussed above. Nonetheless, Figures 10 and 11 show that GBEs are sensitive to the tropospheric precursor field in advance of the stratospheric field, indicating that the troposphere may be leading the stratosphere in Greenland blocking episodes.

7 | DISCUSSION

We have used ensemble sensitivity analysis to quantitatively evaluate the sensitivity of high-latitude blocking over Greenland to two atmospheric precursor fields, specifically Z500 and Z50. Blocking is identified using a two-dimensional blocking index based on reversals in the meridional gradient of Z500, and spatial and temporal constraints are applied to identify events which persist for at least 5 days. Using a prescribed Greenland region results in the identification of 26 GBEs in the ERA-I data for DJF 2006–2015.

The ECMWF TIGGE forecast ensemble of 15-day forecasts is used to conduct ensemble sensitivity analysis of Greenland blocking events. The area-averaged blocking index in a prescribed region about the event maximum for days 2 to 4 after observed onset of a GBE is used as the response function, and the sensitivity of this function to two precursor fields – Z500 and Z50 – is calculated at all forecast lead times. The spread in the response function is thereby related to the spread in the precursor field at some earlier forecast time, highlighting areas of increased sensitivity and allowing the postulation of reasonable dynamical mechanisms for the relationship between the response and precursor fields.

A case-study of a GBE is chosen to illustrate the composite results, using only the 10-day forecast. The model is able to accurately reproduce the Z500 and Z50 precursor fields for 2 to 4 days prior to GBE onset, although the Z50 results exhibit the cold stratospheric bias seen in the composite ensemble mean. A timeline of the 2D blocking index for the reanalysis and the ensemble forecasts shows that the observed index is contained within the ensemble spread, illustrating the ability of the ensemble to model realistic possible forecast states. The evolution of the NAO index prior and subsequent to GBE onset shows a strongly negative NAO for this case, which coincided with the onset of a persistently NAO– period. The MJO phase plot shows phase 6 prior to GBE onset, which has been identified as a possible precursor to NAO– over the eastern Pacific.

A comparison of the composite anomalies in Z500 between the ERA-I reanalysis and the ECMWF ensemble mean show that the model is capable of reproducing the tropospheric precursors to GBEs at lead times of both 10 and 5 days prior to onset. A wave train extends from the Pacific Ocean over North America and into the Atlantic 2 to 4 days prior to GBE onset. The wave 2-type pattern seen in the reanalysis composites for Z50 is somewhat evident in the ensemble means for the 5-day forecast, but absent in the 10-day forecast. The observed strengthening of the Aleutian high is not well reproduced, and the model also exhibits a widespread cold stratospheric bias which develops very early in the forecast.

For 4 and 2 days prior to GBE onset, the patterns of sensitivity are qualitatively similar to the pattern of the Z500 precursors for both the 10- and 5-day forecasts. Regions of sensitivity extend across much of the hemisphere, highlighting the globally connected nature of the dynamics of these events. Some of the local signals may arise as a consequence of the developing GBE. For both forecast lead times, statistically significant at the 95% level sensitivities demonstrate the robustness of the sensitivities in regions where precursors to GBEs have been identified and where the sensitivities are largest in value, indicating that GBEs are more often sensitive to the Tropics than to the Arctic. Comparisons of sensitivity to low- and high-frequency components of Z500 for the 10-day forecast reveal that the spread in Greenland blocking is mostly due to the low-frequency dynamics, with evidence of a wave precursor in the tropical Pacific. The patterns of spread between members are clearer in the 10-day forecasts analysed, but importantly our conclusions are also supported by analysis of the 5-day forecasts in which the model is more closely constrained by the observed initial conditions.

The results for Z50 must be interpreted in the light of probable sensitivity to the cold tropospheric bias in the forecast. There are widespread regions of negative sensitivity over the central Pacific at midlatitudes, the eastern tropical Pacific, and the North Atlantic storm track. Positive sensitivities are largely confined to the polar regions. Fewer events show statistically significant sensitivity to Z50 at high latitudes than for Z500. The comparison of the percentage of episodes with uncorrected sensitivities for Z500 and Z50 shows that GBEs are sensitive to the tropospheric precursor field in advance of the stratospheric field.

The greater sensitivity of GBEs, and hence the negative phase of the NAO, to tropospheric precursors over the tropical Pacific and in the region of the precursor wave train extending from the Pacific Ocean across North America and into the Atlantic, indicates that dynamical processes related to the formation of the wave train may be of importance in the prediction of GBE onset at short forecast lead times. The representation in the forecast model of processes such as tropical convection, which may in turn be related to the MJO, are likely to be of importance. Although some studies suggest that retrogression of existing blocking systems from Northern Europe may be a factor in Greenland blocking onset, this does not appear as a strong factor in the sensitivity analysis of this event set. This does not imply that this process is not acting, but that it is not a dominant source of spread in the forecast ensemble at these time-scales. The cold stratospheric bias evident in the model is also worthy of examination. Although the ensemble sensitivity results indicate that lower stratospheric heights at mid to low latitudes will increase blocking in the Greenland region, which could be interpreted as likely to improve the representation of blocking in the model, the sensitivity may in fact represent ensemble sensitivity to the bias itself – and thus the stratospheric sensitivity results must be interpreted with this in mind.

This study has used a state-of-the-art forecast system and a novel sensitivity method to identify possible sources of forecast spread in the short-term prediction of blocking onset at high latitudes over Greenland. Much of the previous work on this topic has used much simpler idealized models, or observations. Our approach in turn provides the potential to learn about the evolution and predictability of the NAO, with important implications for the evaluation of the likelihood of storm track shifts which may in turn impact precipitation and temperatures over the United Kingdom and Europe. The main conclusion of this paper is that Greenland blocking is sensitive to hemispheric, low-frequency dynamics, in particular, but not exclusively, via a Rossby wave train from the tropical Pacific. Whilst the literature has suggested that the negative phase of the NAO develops locally, this study has shown that NAO– is sensitive to hemispheric precursors, implying greater potential for predictability than might have been expected. These dynamics are well captured by the forecast model 5 days in advance and are also apparent in forecasts initiated 10 days in advance, but the signals are weaker and the occurrence of blocking is lower. It is not clear from this analysis how much this is due to model error or to intrinsically lower predictability of the atmosphere at longer lead times.

ACKNOWLEDGEMENTS

This work was supported by the UK Natural Environment Research Council (grant number NE/L01047X/1). The authors are grateful to the ECMWF for providing the ensemble forecast data via the TIGGE data archive portal. The authors thank the anonymous reviewers for their helpful comments.

REFERENCES

Ancell, B. and Hakim, G.J. (2007) Comparing adjoint- and ensemble-sensitivity analysis with applications to observation targeting. *Monthly Weather Review*, 135, 4117–4134. https://doi.org/10.1175/2007MWR1904.1.

Andrews, D.G. and McIntyre, M.E. (1976) Planetary waves in horizontal and vertical shear: the generalized Eliassen–Palm relation and the mean zonal acceleration. *Journal of the Atmospheric Sciences*, 33, 2031–2048. https://doi.org/10.1175/1520-0469(1976)033<2031:PWIHAV>2.0CO;2.

Athanasiadis, P.J., Wallace, J.M. and Wettstein, J.J. (2009) Patterns of wintertime jet stream variability and their relation to the storm tracks. *Journal of the Atmospheric Sciences*, 67, 1361–1381. https://doi.org/10.1175/2009JAS3270.1.

Baldwin, M.P. and Dunkerton, T.J. (2001) Stratospheric harbinger of anomalous weather regimes. *Science*, 294, 581–584. https://doi.org/10.1126/science.1063315.

Baldwin, M.P., Stephenson, D.B., Thompson, D.W.J., Dunkerton, T.J., Charlton, A.J. and O'Neill, A. (2003) Stratospheric memory and skill of extended-range weather forecasts. *Science*, 301, 636–640. https://doi.org/10.1126/science.1087143.

Barriopedro, D., Garcia-Herrera, R. and Trigo, R.M. (2010) Application of blocking diagnosis methods to general circulation models. Part I: a novel detection scheme. *Climate Dynamics*, 35, 1373–1391. https://doi.org/10.1007/s00382-010-0767-5.

Berrisford, P., Hoskins, B.J. and Tyrlis, E. (2007) Blocking and Rossby wave breaking on the dynamical tropopause in the Southern Hemisphere. *Journal of the Atmospheric Sciences*, 64, 2881–2898. https://doi.org/10.1175/JAS3984.1.

Bougeault, P., Toth, Z., Bishop, C., Brown, B., Burridge, D., Chen, D., Ebert, E., Fuentes, M., Hammil, T., Mylne, K., Nicolau, J., Paccagnella, T., Park, Y.Y., Parsons, D., Raoult, B., Schuster, D., Silva Dias, P., Swinbank, R., Takeuchi, Y., Tennant, W., Wilson, L. and Worley, S. (2010) The THORPEX interactive grand global ensemble. *Bulletin of the American Meteorological Society*, 91, 1059–1072. https://doi.org/10.1175/2010BAMS2853.1.

Buizza, R. and Leutbecher, M. (2015) The forecast skill horizon. *Quarterly Journal of the Royal Meteorological Society*, 141, 3366–3382. https://doi.org/10.1002/qj.2619.

Buizza, R., Leutbecher, M. and Isaksen, L. (2008) Potential use of an ensemble of analyses in the ECMWF ensemble prediction system. *Quarterly Journal of the Royal Meteorological Society*, 134, 2051–2066. https://doi.org/10.1002/qj.346.

Butler, A.H., Sjober, J.P., Seidel, D.J. and Rosenlof, K.H. (2017) A sudden stratospheric warming compendium. *Earth System Science Data*, 9, 63–76. https://doi.org/10.5194/essd-9-63-2017.

Cassou, C. (2008) Intraseasonal interaction between the Madden–Julian Oscillation and the North Atlantic Oscillation. *Nature Letters*, 455, 523–527. https://doi.org/10.1038/nature07286.

Castanheira, J.M. and Barriopedro, D. (2010) Dynamical connection between tropospheric blockings and stratospheric polar vortex. *Geophysical Research Letters*, 37, L13809. https://doi.org/10.1029/2010GL043819.

Cattiaux, J., Yiou, P. and Vautard, R. (2012) Dynamics of future seasonal temperature trends and extremes in Europe: a multi-model analysis from CMIP3. *Climate Dynamics*, 38, 1949–1964. https://doi.org/10.1007/s00382-011-1211-1.

Charlton, A.J. and Polvani, L.M. (2007) A new look at stratospheric sudden warmings. *Journal of Climate*, 20, 449–469. https://doi.org/10.1175/JCLI3996.1.

Cheng, X. and Wallace, J.M. (1993) Cluster analysis of the Northern Hemisphere wintertime 500 hPa height field: spatial patterns. *Journal of the Atmospheric Sciences*, 50, 2674–2696. https://doi.org/10.1175/1520-0469(1993)050<2674:CAOTNH>2.0.CO;2.

Croci-Maspoli, M., Schwierz, C. and Davies, H.C. (2007) Atmospheric blocking: space–time links to the NAO and PNA. *Climate Dynamics*, 29, 713–725. https://doi.org/10.1007/s00382-007-0259-4.

Dacre, H.F. and Gray, S.L. (2015) Quantifying the climatological relationship between extratropical cyclone intensity and atmospheric precursors. *Geophysical Research Letters*, 40, 2322–2327. https://doi.org/10.1002/grl.50105.

Davini, P., Cagnazzo, C. and Anstey, J.A. (2014) A blocking view of the stratosphere–troposphere coupling. *Journal of Geophysical Research – Atmospheres*, 119(19), 11100–11115. https://doi.org/10.1002/2014JD021703.

Dee, D.P., Uppala, S.M., Simmons, A.J., Berrisford, P., Poli, P., Kobayashi, S., Andrae, U., Balmaseda, M.A., Balsamo, G., Bauer, P., Bechtold, P., Beljaars, A.C.M., van de Berg, L., Bidlot, J., Bormann, N., Delsol, C., Dragani, R., Fuentes, M., Geer, A.J., Haimberger, L., Healy, S.B., Hersbach, H., Hólm, E.V., Isaksen, L., Kållberg, P., K'ohler, M., Matricardi, M., McNally, A.P., Monge-Sanz, B.M., Morcrette, J.-J., Park, B.-K., Peubey, C., de Rosnay, P., Tavolato, C., Thépaut, J-N and Vitart, F. (2011) The ERA-Interim reanalysis: configuration and performance of the data assimilation system. *Quarterly Journal of the Royal Meteorological Society*, 137, 553–597. https://doi.org/10.1002/qj.828.

Diao, Y., Li, J. and Luo, D. (2006) A new blocking index and its application: blocking action in the Northern Hemisphere. *Journal of Climate*, 19, 4819–4839. https://doi.org/10.1175/JCLI3886.1.

Drouard, M., Rivière, G. and Arbogast, P. (2015) The link between the North Pacific climate variability and the North Atlantic Oscillation via downstream propagation of synoptic waves. *Journal of Climate*, 28, 3957–3976. https://doi.org/10.1175/JCLI-D-14-00552.1.

Efthymiadis, D., Goodess, C.M. and Jones, P.D. (2011) Trends in Mediterranean gridded temperature extremes and large-scale circulation influences. *Natural Hazards and Earth System Sciences*, 11, 2199–2214. https://doi.org/10.5194/nhess-11-2199-2011.

Feldstein, S.B. (1976) The dynamics of NAO teleconnection pattern growth and decay. *Quarterly Journal of the Royal Meteorological Society*, 129, 901–924. https://doi.org/10.1256/qj.02.76.

Ferranti, L., Corti, S. and Janousek, M. (2015) Flow-dependent verification of the ECMWF ensemble over the Euro-Atlantic sector. *Quarterly Journal of the Royal Meteorological Society*, 141, 916–924. https://doi.org/10.1002/qj.2411.

Frame, T.H.A., Ambaum, M.H.P., Gray, S.L. and Methven, J. (2011) Ensemble prediction of transitions of the North Atlantic eddy-driven jet. *Quarterly Journal of the Royal Meteorological Society*, 137, 1288–1297. https://doi.org/10.1002/qj.829.

Frame, T.H.A., Methven, J., Gray, S.L. and Ambaum, M.H.P. (2013) Flow-dependent predictability of the North Atlantic jet. *Geophysical Research Letters*, 40, 2411–2416. https://doi.org/10.1002/grl.50454.

Franzke, C., Lee, S. and Feldstein, S.B. (2004) Is the North Atlantic Oscillation a breaking wave?. *Journal of the Atmospheric Sciences*, 61, 145–160. https://doi.org/10.1175/1520-0469(2004)061<0145:ITNAOA>2.0.CO;2.

Garcies, L. and Homar, V. (2009) Ensemble sensitivities of the real atmosphere: application to Mediterranean intense cyclones. *Tellus*, 61A, 394–406. https://doi.org/10.1111/j.1600-0870.2009.00392.x.

Gollan, G., Greatbach, R.J. and Jung, T. (2015) Origin of variability in Northern Hemisphere winter blocking on interannual to decadal timescales. *Geophysical Research Letters*, 42, 10037–10046. https://doi.org/10.1002/2015GL066572.

Hakim, G.J. and Torn, R.D. (2008) Ensemble synoptic analysis. In *Synoptic Dynamic Meteorology and Weather Analysis and Forecasting. A Tribute to Fred Sanders.* Bosart, L.F., Bluestein (Ed.), American Meteorological Society, Boston, MA.

Henderson, S.A., Maloney, E.D. and Barnes, E.A. (2016) The influence of the Madden–Julian Oscillation on Northern Hemisphere winter blocking. *Journal of Climate*, 29, 4597–4616. https://doi.org/10.1175/JCLI-D-15-0502.1.

Hurrell, J.W. and Deser, C. (2009) North Atlantic climate variability: the role of the North Atlantic Oscillation.. *Journal of Marine Systems*, 78, 28–41. https://doi.org/10.1016/j.jmarsys.2008.11.026.

Hurrell, J.W., Kushnir, Y., Ottersen, G. and Visbeck, M. (2003) An overview of the North Atlantic Oscillation. In *The North Atlantic Oscillation: Climatic Significance and Environmental Impact,* Geophysical Monograph 134. Hurrell, J.W, Kushnir, Y, Ottersen, G, Visbeck, M (Eds). American Geophysical Union, Washington, DC.

Jung, T., Kasper, M.A., Semmler, T. and Serrar, S. (2014) Arctic influence on subseasonal midlatitude prediction. *Geophysical Research Letters*, 41, 2676–3680. https://doi.org/10.1002/2014GL059961.

Kelly, G., Thépaut, J.-N., Buizza, R. and Cardinali, C. (2007) The value of observations. I: data denial experiments for the Atlantic and the Pacific. *Quarterly Journal of the Royal Meteorological Society*, 133, 1803–1815. https://doi.org/10.1002/qj150.

Kenyon, J. and Hegerl, G.C. (2010) Influence of modes of climate variability on global precipitation extremes. *Journal of Climate*, 23, 6248–6262. https://doi.org/10.1175/2010JCLI3617.1.

Kimoto, M. and Ghil, M. (1993) Multiple flow regimes in the Northern Hemisphere winter. Part I: methodology and hemispheric regimes. *Journal of the Atmospheric Sciences*, 50, 2625–2643. https://doi.org/10.1175/1520-0469(1993)050$<$3C2625:MFRITN$>$3E2.0.CO;2.

Lawrence, B.N., Bennett, V.L., Churchill, J., Juckes, M., Kershaw, P., Pascoe, S., Pepler, S., Pritchard, M. and Stephens, A. (2013) Storing and manipulating environmental big data with JASMIN. In: *2013 IEEE International Conference on Big Data*, 6–9 October 2013, Silicon Valley, CA, USA.

Limpasuvan, V., Thompson, D.W.J. and Hartmann, D.L. (2004) The life cycle of Northern Hemisphere sudden stratospheric warmings. *Journal of Climate*, 17, 2584–2596. https://doi.org/10.1175/1520-0442(2004)017$<$2584:TLCOTN$>$2.0.CO;2.

Lin, H., Brunet, G. and Fontecilla, J.S. (2010) Impact of the Madden–Julian Oscillation on the intraseasonal forecast skill of the North Atlantic Oscillation. *Geophysical Research Letters*, 37, L19803. https://doi.org/10.1029/2010GL044315.

Luo, D., Cha, J., Zhong, L. and Dai, A. (2014) A nonlinear multi-scale interaction model for atmospheric blocking: the eddy-blocking matching mechanism. *Quarterly Journal of the Royal Meteorological Society*, 140, 1785–1808. https://doi.org/10.1002/qj.2337.

Luo, D., Lupo, A.R. and Wan, H. (2007) Dynamics of eddy-driven low-frequency dipole modes. Part I: a simple model of North Atlantic Oscillations. *Journal of the Atmospheric Sciences*, 64, 3–28. https://doi.org/10.1175/JAS3818.1.

Luo, D., Yao, Y. and Dai, A. (2015) Decadal relationship between European blocking and the North Atlantic Oscillation during 1978-2011. Part II: a theoretical model study. *Journal of the Atmospheric Sciences*, 64, 3–28. https://doi.org/10.1175/JAS-D-14-0040.1.

Magnusson, L. (2017) Diagnostic methods for understanding the origin of forecast errors. *Quarterly Journal of the Royal Meteorological Society*, 143, 2129–2142. https://doi.org/10.1002/qj.3072.

Marsh, T.J., Parry, S., Kendon, M.C. and Hannaford, J. (2013) *The 2010–2012 drought and subsequent extensive flooding*. Centre for Ecology & Hydrology, Wallingford, UK.

Martius, O., Polvani, L.M. and Davies, H.C. (2009) Blocking precursors to stratospheric sudden warming events. *Geophysical Research Letters*, 36, L14806. https://doi.org/10.1029/2009GL038776.

Masato, G., Hoskins, B.J. and Woollings, T.J. (2013a) Wave-breaking characteristics of Northern Hemisphere winter blocking: a two-dimensional approach. *Journal of Climate*, 26, 4535–4549. https://doi.org/10.1175/JCLI-D-12-00240.1.

Masato, G., Hoskins, B.J. and Woollings, T.J. (2013b) Winter and summer Northern Hemisphere blocking in CMIP5 models. *Journal of Climate*, 26, 7044–7059. https://doi.org/10.1175/JCLI-D-12-00466.1.

Matsueda, M. (2009) Blocking predictability in operational medium-range ensemble forecasts. *SOLA*, 5, 113–116. https://doi.org/10.2151/sola.2009-029.

Mauritsen, T. and Källén, E. (2004) Blocking prediction in an ensemble forecasting system. *Tellus*, 56A, 218–228. https://doi.org/10.3402/tellusa.v56i3.14411.

Mitchell, D.M., Gray, L.J., Anstey, J., Baldwin, M.P. and Charlton-Perez, A.J. (2012) The influence of stratospheric vortex diplacements and splits on surface climate. *Journal of Climate*, 26, 2668–2682. https://doi.org/10.1175/JCLI-D-12-00030.1.

Mukougawa, H. and Hirooka, T. (2004) Predictability of stratospheric sudden warming. *Monthly Weather Review*, 132, 1764–1776. https://doi.org/10.1175/1520-0493(2004)132<1764:POSSWA>2.0.CO;.

Nakamura, H. and Anderson, J.L. (1997) The role of high- and low-frequency dynamics in blocking formation. *Monthly Weather Review*, 125, 2074–2093. https://doi.org/10.1175/1520-0493(1997)125<2074:TROHAL>2.0.CO;2.

Nishii, K., Nakamura, H. and Orsolini, Y.J. (2011) Geographical dependence observed in blocking high influence on the stratospheric variability through enhancement and suppression of upward planetary-wave propagation. *Journal of Climate*, 24, 6408–6423. https://doi.org/10.1175/JCLI-D-10-0502.1.

O'Neill, A. and Taylor, B.F. (1979) A study of the major stratospheric warming of 1976/77. *Quarterly Journal of the Royal Meteorological Society*, 105, 71–92. https://doi.org/10.1002/qj.49710544306/full.

Oortwijn, J. (1998) Predictability of the onset of blocking and strong zonal flow regimes. *Journal of the Atmospheric Sciences*, 55, 973–994. https://doi.org/10.1175/1520-0469(1998)055$<$0973:POTOOB$>$2.0.CO;2.

Palmer, T.N., Buizza, R., Doblas-Reyes, F.J., Jung, T., Leutbecher, M., Shutts, G.J., Steinheimer, M. and Weisheimer, A. (2009) Stochastic Parametrization and Model Uncertainty. Technical Memorandum 598, ECMWF, Reading, UK.

Pelly, J.L. and Hoskins, B.J. (2003a) A new perspective on blocking. *Journal of the Atmospheric Sciences*, 60, 743–755. https://doi.org/10.1175/1520-0469(2003)060$<$0743:ANPOB$>$2.0.CO.

Pelly, J.L. and Hoskins, B.J. (2003b) How well does the ECMWF ensemble prediction system predict blocking?. *Quarterly Journal of the Royal Meteorological Society*, 129, 1683–1702. https://doi.org/10.1256/qj.01.173.

Pfahl, S., Schwierz, C., Croci-Maspoli, M., Grams, M. and Wernli, H. (2015) Importance of latent heat release in ascending air streams for atmospheric blocking. *Nature Geoscience*, 8, 610–614. https://doi.org/10.1038/ngeo2487.

Rodwell, M.J., Magnusson, L., Bauer, P., Bechtold, P., Bonavita, M., Carinali, C., Diamantakis, M., Earnshaw, P., Garcia-Mendez, A., Isaksen, L., Källén, E., Klocke, D., Lopez, P., McNally, A.P., Persson, A., Prates, F. and Wedi, N. (2013) Characteristics of occasional poor medium-range weather forecasts for Europe. *Bulletin of the American Meteorological Society*, 94, 1393–1405. https://doi.org/10.1175/BAMS-D-12-00099.1.

Rivière, G. and Orlanski, I. (2007) Characteristics of the Atlantic storm track eddy activity and its relationship with the North Atlantic Oscillation. *Journal of Atmospheric Sciences*, 64, 241–266. https://doi.org/10.1175/JAS3850.1.

Santos, J.A., Corte-Real, J. and Leite, S. (2007) Atmospheric large-scale dynamics during the 2004/2005 winter drought in Portugal. *International Journal of Climatology*, 27, 571–586. https://doi.org/10.1002/joc.1425/pdf.

Santos, J.A., Woollings, T. and Pinto, J.G. (2013) Are the winters 2010 and 2012 archetypes exhibiting extreme opposite behaviour of the North Atlantic jet stream?. *Monthly Weather Review*, 141, 3626–3640. https://doi.org/10.1175/MWR-D-13-00024.1.

Sardeshmukh, P.D. and Hoskins, B.J. (1988) The generation of global rotational flow by steady idealized tropical divergence. *Journal of Atmospheric Sciences*, 45, 1228–1251. https://doi.org/10.1175/1520-0469(1988)045<1228:TGOGRF>2.0CO;2.

Scherrer, S.C., Croci-Maspoli, M., Schwierz, C. and Appenzeller, C. (2006) Two-dimensional indices of atmospheric blocking and their statistical relationship with winter climate patterns in the Euro-Atlantic region. *International Journal of Climatology*, 26, 233–249. https://doi.org/10.1002/joc.1250.

Schwierz, C., Croci-Maspoli, M. and Davies, H.C. (2004) Perspicacious indicators of atmospheric blocking. *Geophysical Research Letters*, 31, L06125. https://doi.org/10.1029/2003GL019341.

Shabbar, A., Huang, J. and Higuchi, K. (2001) The relationship between the wintertime North Atlantic Oscillation and blocking episodes in the North Atlantic. *International Journal of Climatology*, 21, 355–369. https://doi.org/10.1002/joc.612.

Shutts, G.J., Leutbecher, M., Weisheimer, A., Stockdale, T., Isaksen, L. and Bonavita, M. (2011) Representing model uncertainty: stochastic parametrizations at ECMWF. *ECMWF Newsletter*, 129, 10–24. https://doi.org/10.21957/fbqmkhv7.

Sung, M.-K., Lim, G.-H., Kug, J.-S. and An, S.-I. (2011) A linkage between the North Atlantic Oscillation and its downstream development due to the existence of a blocking ridge. *Journal of Geophysical Research*, 116, D11107. https://doi.org/10.1029/2010JD015006.

Takaya, K. and Nakamura, H. (2001) A formulation of a phase-independent wave-activity flux for stationary and migratory quasi-geostrophic eddies on a zonally varying basic flow. *Journal of Atmospheric Sciences*, 58, 608–627. https://doi.org/10.1175/1520-0469(2001)058<0608:AFOAPI>2.0CO;2.

Thompson, D.W.J. and Wallace, J.M. (2001) Regional climate impacts of the Northern Hemisphere annular mode. *Science*, 293, 85–89. https://doi.org/10.1126/science.1058958.

Tibaldi, S. and Molteni, F. (1990) On the operational predictability of blocking. *Tellus*, 42A, 343–365. https://doi.org/10.1034/j.1600-0870.1990.t01-2-00003.x.

Tibaldi, S., Tosi, E., Navarra, A. and Pedulli, L. (1994) Northern and Southern Hemisphere seasonal variability of blocking frequency and predictability. *Monthly Weather Review*, 122, 1971–2003. https://doi.org/10/1175/1520-0493(1994)122<1972:NASHSV>2.0.CO;2.

Torn, R.D. and Hakim, G.J. (2008) Ensemble-based sensitivity analysis. *Monthly Weather Review*, 136, 663–677. https://doi.org/10.1175/2007MWR2132.1.

Torn, R.D., Whitaker, J.S., Pegion, P., Hamill, T.M. and Hakim, G.J. (2015) Diagnosis of the source of GFS medium-range track errors in hurricane *Sandy* (2012). *Monthly Weather Review*, 143, 132–152. https://doi.org/10.1175/MWR-D-14-00086.1.

Trigo, R.M., Pozo-Vàzquez, D., Osborn, T.J., Castro-Díez, Y., Gámiz-Fortis, S. and Esteban-Parra, M.J. (2004) North Atlantic Oscillation influence on precipitation, river flow and water resources in the Iberian Peninsula. *International Journal of Climatology*, 24, 925–944. https://doi.org/10.1002/joc.1048.

Tyrlis, E. and Hoskins, B.J. (2008) Aspects of Northern Hemisphere atmosperic blocking climatology. *Journal of Atmospheric Sciences*, 65, 1638–1652. https://doi.org/10.1175/2007JAS2337.1.

Vautard, R. (1990) Multiple weather regimes over the North Atlantic: analysis of precursors and successors. *Monthly Weather Review*, 118, 2056–2081. https://doi.org/10.1175/1520-0493(1990)118<2056:MWROTN>2.0.

Vitart, F., Balsamo, G., Buizza, R., Ferranti, L., Keeley, S., Magnusson, L., Molteni, F. and Weisheimer, A. (2014) Sub-seasonal predictions. Technical Memorandum 734, ECMWF, Reading, UK.

Wallace, J.M., Lim, G.-H. and Blackmon, M.L. (1988) Relationship between cyclone tracks, anticyclone tracks, and baroclinic waveguides. *Journal of Atmospheric Sciences*, 45, 439–462. https://doi.org/10.1175/1520-0469(1988)045$<$0439:RBCTAT$>$2.0.CO;2.

Wanner, H., Brönniman, S., Casty, C., Gyalistras, D., Luterbacher, J., Schmutz, C., Stephenson, D.B. and Xoplaki, E. (2001) North Atlantic Oscillation – Concepts and studies. *Surveys in Geophysics*, 22, 321–382. https://doi.org/10.1023/A:1014217317898.

Watson, J.C. and Colucci, S. (2002) Evaluation of ensemble predictions of blocking in the NCEP global spectral model. *Monthly Weather Review*, 130, 3008–3021. https://doi.org/10.1175/1520-0493(2002)130<3008:EOPOB>2.0C;2.

Woollings, T. and Hoskins, B.J. (2008) Simultaneous Atlantic–Pacific blockings and the Northern Annular Mode. *Quarterly Journal of the Meteorological Society*, 134, 1635–1646. https://doi.org/10.1002/qj.310.

Woollings, T., Hoskins, B.J., Blackburn, M. and Berrisford, P. (2008) A new Rossby wave-breaking interpretation of the North Atlantic Oscillation. *Journal of the Atmospheric Sciences*, 65, 609–626. https://doi.org/10.1175/2007JAS2347.1.

Woollings, T., Charlton-Perez, A., Ineson, S., Marshall, A.G. and Masato, G. (2010) Associations between stratospheric variability and tropospheric blocking. *Journal of Geophysical Research – Atmospheres*, 115, D06108. https://doi.org/10.1029/2009JD012742.

How to cite this article: Parker T, Woollings T, Weisheimer A. Ensemble sensitivity analysis of Greenland blocking in medium-range forecasts. *Q J R Meteorol Soc.* 2018;144:2358–2379. https://doi.org/10.1002/qj.3391